Department of Mechanical Engineering
2018-06-088 | Version 1.1

Fluid mechanic causes of gas migration

Final Report for PTAC-16-WARI-02 & BCOGRIS project EI-2016-09

Ian A. Frigaard

Parts of this research have been conducted using funding from the following organizations, to whom we express our sincere appreciation:

THE UNIVERSITY OF BRITISH COLUMBIA

Fluid Mechanic Causes of Gas Migration

Fluid Mechanic Causes of Gas Migration 2

Executive Summary 3

Problem 1: Micro-annulus formation during mud removal *4*
Problem 2: Fluids invasion *5*

Best Practices Recommendations 6

Tangible Project Outcomes 8

Background 10

Problem 1: Micro-annulus formation during mud removal 14

Methodology *14*
Results and Data *15*
Density stable displacements 15
Density unstable displacements 19
Discussion & Conclusions *27*

Problem 2: Fluids invasion 32

Methodology *32*
Results and Data *35*
Miscible invasion 35
Immiscible invasion 39
Discussion and Conclusions *42*

Recommendations 46

Application and Dissemination of Results 47

References: 49

Executive Summary

This is a final report for work on the project “Fluid Mechanic Causes of Gas Migration”, which has been conducted at the University of British Columbia, Department of Mechanical Engineering, primarily by Ms Marjan Zare under the supervision of Prof Ian Frigaard. This work forms the main part of the PhD thesis of M. Zare, (due to be examined in Summer 2018), which will then be a publicly available permanent record of the research.

This work has been funded by the Alberta Upstream Petroleum Research Fund Program (AUPRF) through PTAC (project number PTAC-16-WARI-02), from October 1st 2016 to June 30 2018. The work continued a research project of the same name funded by BCOGRIS (project number EI-2016-09), from October 1st 2015 to September 30 2016. Earlier work on this project was initiated under a larger collaborative research and development grant between Schlumberger and NSERC (CRD project number 444985-12: “Topics in Oilfield Cementing Fluid Mechanics”), which addressed wider range of technical challenges. M. Zare commenced her PhD studies on the project in 2013.

The project concerns the in depth study of a topic of critical importance to the upstream oil & gas industry: namely the leakage of oil & gas wells. This is a common occurrence worldwide and leakage rates have been reported in the Canadian context by various authors; see Dusterhoft et al (2002), Dusseault et al (2014), Atherton et al (2017). Broadly speaking, an average of 10-20% of wells in Western Canada leak. There appears to be significant variability depending on geology, operational factors and of course the criteria used to define leakage. The concerns are various, depending on the stakeholder: reduced productivity (due to reservoir pressure reduction), environmental (emissions and near-surface ecology), health (groundwater pollution or emitted gas toxicity), public perception, regulatory effectiveness.

Although there are instances of gas detection distant from a wellbore, by far the most common is near-wellbore leakage: through the cemented surface casing (SCVF). This means that pathways exist through the cemented annular gap that are more permeable to reservoir gas than any other pathway from gas source to surface. Although of topical interest, this is not a new phenomenon and has received industrial attention for decades. The complexity arises from the fact that many different physical phenomena and operational procedures can lead to gas migration.

In this project we have selected 3 problem areas of relevance to gas migration, in each of which the underlying process is governed by fluid mechanics.

- **Micro-annulus formation during mud removal**, i.e. are there ways in which drilling fluid is left behind in a thin wall layer, which later dehydrates and forms a migration path for gas?
- **Fluids invasion**: how do fluids actually invade a gelled column of liquid under pressure, i.e. the cement slurry as it begins to hydrate, or even a thick mud layer?
- **Cement hydration**: are there mechanisms occurring during setting of the cement slurry that reduce pressure in the annulus, encouraging fluids to invade and migrate?

The main results achieved in the project concern the first two of these areas and are explained in this report. For the 3rd problem, our results have mainly been in formulating a mathematical model for this complex process, but so far we have not progressed further with results of industrial relevance. This 3rd part will only be documented in the PhD thesis of M. Zare.

Best practices and tangible benefits are summarized in separate sections of this report. Below we explain the main results of problems 1 & 2.

Problem 1: Micro-annulus formation during mud removal

Project 1 gives a concise computational and model based study of the fluid mechanical phenomenon of a wet micro-annulus. This is a layer of drilling mud that is left behind on the walls of the annulus following primary cementing. By concise we mean that the study reduces the dimensionless parameter space from 12 to 4 parameters, which is still complex. The simplification with respect to the annulus is also geometric, in that we consider a long vertical channel which can be interpreted as a longitudinal section of a narrow annulus. The detailed results of the paper are in Zare et al (2017) and Zare & Frigaard (2018b). More than 1000 two-dimensional (2D) detailed computations have been carried out, coupled to simpler models and analysis.

Density stable displacements are most common, i.e. the heavier fluid pushes the lighter fluid upwards. For these we generally see stable flows. Static mud layers are easily found in our simulation study, when the yield stress is strong enough to overcome the combination of buoyancy and frictional stresses. In post-processing our simulations we can compute the residual layer thickness h at the end of the channel. Many of the parametric effects we have observed are intuitive: increasing displacing fluid viscosity improves the displacement, as does increasing the buoyancy force. Counter-intuitive however, is the decrease in h as the yield stress of the drilling mud increases (an effect most evident at small to moderate buoyancy). As well as the thickness h, a critical feature is whether or not the wall layer is moving. This depends on both h and h_{max}, which is the maximal static wall layer thickness. The latter is easily computed for density stable displacement. We have developed various techniques to qualitatively predict mud layer behavior – summarized later in the report. We also have derived conditions under which there can be no wet micro-annulus

Density unstable displacements occur with some lightweight spacer fluids and with washes (although these are often in turbulent flow). The main differences that arise are: (i) a range of hydrodynamic instabilities are found (detailed in the report below); (ii) we find that static mud layers can result even for very low yield stresses. This can happen because buoyancy acts against the mean flow. Thus, with thick enough wall layer and strong enough buoyancy force we are able to have wall shear stresses that are very small. This allows a yield stress fluid to remain static near the wall at smaller yield stresses than would be the case for a density stable displacement. We have observed these layers in our 2D simulations.

We have developed a 1D analysis, similar to that for density stable displacements, which allows us to define a maximal static layer thickness. This is however slightly more complex than the density stable case to compute. We have also been able to develop a 1D analysis that can successfully predict when the more complex 2D flows will be stable or unstable. The hydrodynamically unstable flows we have observed are disappointing from the perspective of mud removal. We had hypothesized that the instabilities would result in thinner residual mud layers, but there is no strong evidence for this in our study. Overall, we feel that density unstable flows do not have any positive effect on wall layers/wet micro-annuli, and probably the reverse. A simple criterion developed for eliminating static wall layers in stable displacements is not valid for density unstable displacements and we must balance the (unproven) potential for destabilization with the demonstrated ability of having partially static residual layers as we increase the buoyancy.

A number of recommended future directions are given later in the report.

Problem 2: Fluids invasion

We have conducted lab-scale experiments targeted at exposing the effects of the yield stress on the (over-)pressure required for one fluid to invade a column of another fluid, through a small hole. This setup was designed to simulate invasion into a well during primary cementing, for relatively low porosity reservoirs where pores may be considered isolated, e.g. in our experiment the hole radius was ~1% of the column radius.

For miscible fluids our results show approximately linear increase in the required over-pressure for invasion, with both the height of fluid column and the yield stress of the invaded fluid column. A number of interesting stages have been identified during the experiments: *mixing*, *invasion*, *transition*, *fracture* and *arrest*. The passage from invasion to transition pressure seems to represent elastic-plastic yielding close to the invasion hole. The initial growth of the transition dome and then slowing of growth (in cases where the fracture does not start immediately) suggests a relaxation of the stress field, due to the over-pressure now being applied over a larger area. We have seen that the expanding dome interface can be either relatively smooth or granular. This does not appear to have any bearing on the stability of the transition dome: either may be stable or unstable. Invasion and transition domes are approximately axisymmetric. Fracture initiation and propagation represent a departure from symmetry, probably due to either a local defect or a non-uniformity of the stress-field.

Our tests with glycerin solutions, comparing against the water invasion studies revealed: (i) the glycerin solutions have a slower mixing/invasion stage (longer times before transition); (ii) invasion pressures are consequently higher; (iii) after transition the invading domes grow more rapidly and are significantly larger than those for water at the point when fracturing initiates. These differences are partly attributed to the larger viscosities of the glycerin, which we believe slows diffusive/mixing processes. On the other hand, there are many similarities to the water invasion studies. The invasion stages are similar and for all miscible fluids tested invasion is a strongly localised process. The increase in invasion pressure with column height is also far slower for miscible fluids than the Poiseuille flow limit would suggest, confirming the local nature of the flow.

Our experiments with immiscible fluids involved a density matched silicon oil (R550) and air. It was immediately apparent that interfacial tension had a large effect on invasion. Our experimental protocol was changed to increase the invasion pressure in larger steps than for the miscible fluids. Mixing was eliminated as was the occurrence of an initial micro-invasion dome. Instead, once invasion started we observe a clear interface expanding into the Carbopol column. In the case of the R550 the interface evolved as an approximately hemispherical dome, slowly filling the bottom of the column. The invasion pressure was significantly larger than for the glycerin solutions and was non-local in that it was resisted by yielding at the walls of the column, increasing as the Poiseuille flow.

The air also did not mix and had no micro-invasion dome. However, the invasion was localised in the sense that buoyancy dominated after any significant influx, leading to the invading fluid stretching upwards into a long bubble, which eventually detached and propagated to the surface. Thus, resistance of invasion at the walls did not occur and the invasion pressure was approximately constant with height of column. Also the measured invasion pressure was much larger for air than for R550. Further analysis of this increased invasion pressure suggested that about 50\% of the increase is directly attributable to interfacial tension and the remainder to yield stress. However, the yield stress is only able to resist effectively when there is no mixing/diffusion.

A number of interesting avenues suggest themselves for future work in this area, outlined in the recommendations section.

Background

A simplified summary of gas migration is given by Nelson & Guillot (2006). They assert that 3 factors must be present in order for gas migration to occur: there needs to be a driving pressure, a space to enter the annulus and a path for the fluids to migrate. Although over-simplistic, this represents a useful conceptual framework.

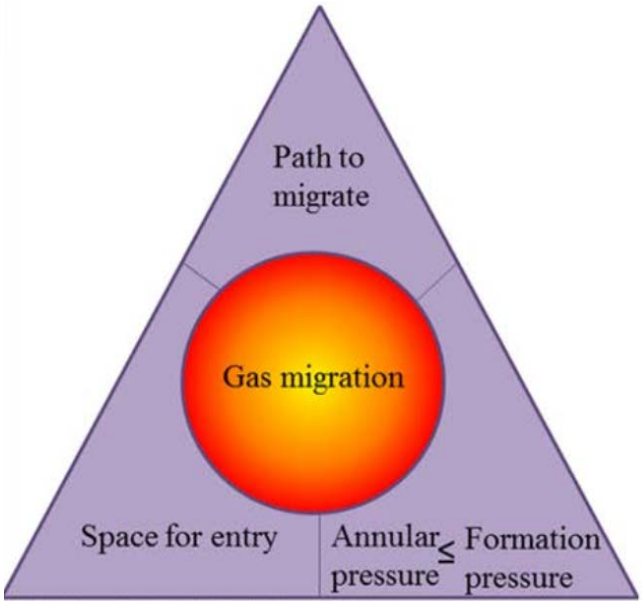

Figure 1: Conditions required for gas migration; from Nelson & Guillot (2006)

One issue with Figure 1 is that there is no indication of mechanism. In practice there are many potential causes of gas migration along cemented casings. These causes are reviewed, along with possible remedies, by Bonett & Pafitis (1996). Some are illustrated below in Figure 2. One popular method of categorizing these causes has been temporal. Immediate and short term gas migration refers to those causes that arise during and just after placement. Medium and longer term migration refer to processes that occur after the initial cement hydration. An example of a long term cause would include stress-induced cracking, e.g. due to geo-mechanical causes or thermal cycling.

An immediate/short term cause could include having the wrong density slurry (inducing invasion) or failing to remove the drilling mud adequately. Both these are fluid mechanic causes, but note that their consequence could lead to other phenomena illustrated above. For example, residual drilling mud in the annulus after placement could be in the form of a mud channel on the narrow side, or a wet micro-annulus (layers on the walls), or trapped in washouts or other weak formation structures. Any of these might lead to contamination, affecting the set cement permeability. The mud layers/channel might also dehydrate as water is consumed by the setting slurry, leaving porous conduits along the annulus. Although the mud channel cause is immediate/short term, gas migration might occur on the medium/long term.

Equally a mud layer means poor interfacial bonding, but poor bonding can also result from shrinkage, mechanical deformation or perhaps even later operational factors such as hydraulic fracturing or high pressure squeeze cementing operations, i.e. anything which may induce deformation of the casing and cement. Note that mechanical bonding, i.e. holding the casing in place is different from the interfacial bond required to seal hydraulically.

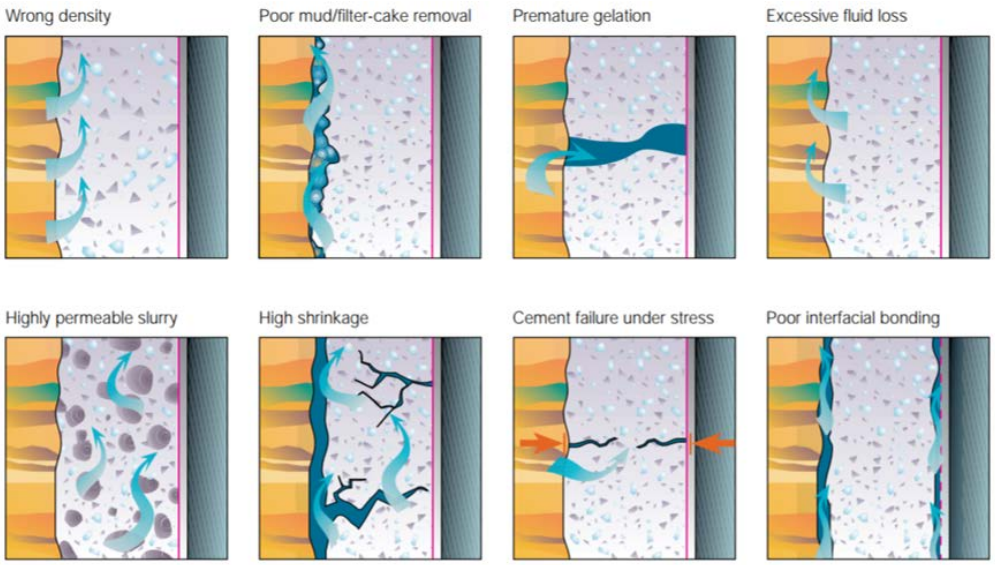

□*Major contributing parameters during the cementing process, in the order that they typically occur. Incorrect cement densities can result in hydrostatic imbalance. Poor mud and filter-cake removal leaves a route for gas to flow up the annulus. Premature gelation leads to loss of hydrostatic pressure control. Excessive fluid loss contributes to available space in the cement slurry column for gas to enter. Highly permeable slurries result in poor zonal isolation and offer little resistance to gas flow. High cement shrinkage leads to increased porosity and stresses in the cement sheath that may cause a microannulus to form. Cement failure under stress helps gas fracture cement sheaths. Poor bonding can cause failure at cement-casing or cement-formation interfaces.*

Figure 2: Illustration of contributing factors to gas migration; from Bonett & Pafitis (1996).

It is due to the complexity discussed above that we have focused this research on understanding key physical phenomena that underlie causes of gas migration. Causally, we have restricted this to fluid mechanics, i.e. rather than target the end effect, so that any insights might help eliminate these causes.

The two projects we have addressed consider: (i) the mechanisms by which a stationary wall layer of drilling mud is left behind during the primary cementing operation (Problem 1), illustrated in 2 of the subfigures of Figure 2 (poor mud removal and poor interfacial bonding); (ii) the mechanism by which a fluid invades a gelled column (Problem 2), also illustrated in 2 of the subfigures of Figure 2 (wrong density and premature gelation).

For problem 1, if we were to consider the displacement flow of drilling mud from a uniform eccentric annulus in its full generality the physical problem is described by the local well inclination, 2 radii, an eccentricity, gravitational acceleration, either molecular diffusivity or interfacial tension, a flow rate and the properties of the 2 fluids which are generally characterized as Herschel-Bulkley fluids (6 rheological parameters, 2 densities). This is a total of 15 parameters which may be reduced to 12 dimensionless parameters following scaling. Unless the model is simple and quick, running any model and analyzing results meaningfully over a 12-dimensional fluid-dynamical design space is prohibitive in terms of time and complexity, not only for the researcher but also to communicate results to industry in a way that is understandable and applicable.

For the above reason, we have limited the scope of our study in the following ways:

a. In terms of well leakage the surface casing is perhaps the most critical. The top of the well is typically vertical and the diameter is largest, while the mean annular gap does not vary much with successive casings. Thus, the surface casing has the smallest aspect ratio of gap width to circumference and in a

vertical well azimuthal buoyancy forces and related azimuthal flows are minimized. In these situations we can model a longitudinal section of the annulus by a vertical plane channel.

b. Our main focus is on static residual wall layers. Fluids without a yield stress will be removed from the walls (albeit slowly if very viscous or due to capillary/wetting effects), so in order to have persistent wall layers we need for the displaced fluid (drilling mud) to have a yield stress. The two fluids may also have different viscosities in field applications and broadly speaking this is a property that we might consider in fluids design. Although the fluids are shear-thinning, the main contribution of this is to an effective viscosity. Consequently, we simplify by having only a Newtonian fluid displacing a Bingham fluid.

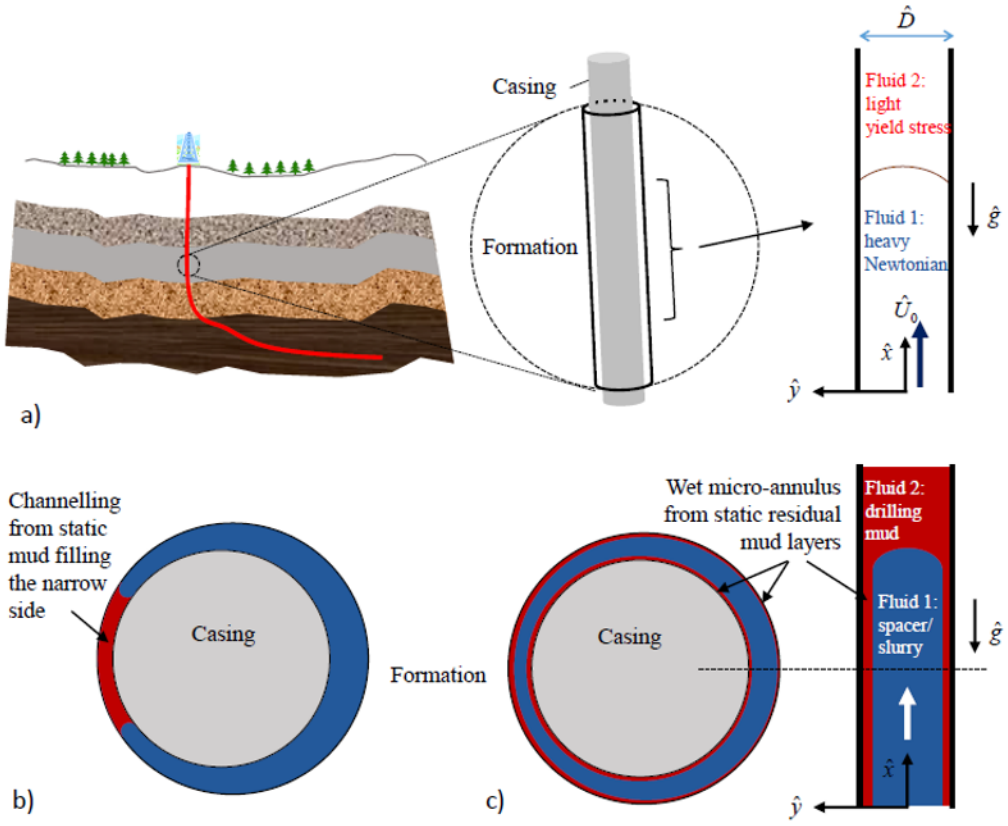

Figure 3: Problem 1 background and simplification. a) Shows the narrow annulus approximation as a plane channel displacement for surface casing (here illustrated with a density stable configuration). b) A static mud channel on the narrow side of the annulus (not studied). c) The phenomena of a wet micro-annulus, resulting from poor fluid displacement.

c. Two other assumptions are also made: the Boussinesq approximation (limiting density effects to the generation of buoyancy forces) and the large Péclet number approximation (meaning that *molecular* diffusion between fluids is not significant in a typical cementing job). The large Péclet number approximation means that these flows are equivalent to large capillary number flows.

The above 3 assumptions reduce to 4 the number of dimensionless groups that must be considered, which is more feasible to study. The physical effects of all the 15 different process parameters can be simulated through their effects on these 4 dimensionless parameters. A schematic showing the background to problem 1 is shown in Figure 3. We study both density stable and density unstable displacement flows. Although the cement slurry and most

spacer fluids are denser than drilling muds, washes and lightweight spacers are less dense. Equally, viscosity ratios between displacing and displaced fluid can be >1 or <1. This constitutes the industrial background to problem 1. The academic/scientific background is given in detail in Zare et al (2017), Zare & Frigaard (2018b).

For problem 2 we return to the schematic of Figure 1 with a more critical eye. Certainly there needs to be a driving force for invasion and a positive pressure differential is the key factor. However, a positive pressure differential might not be sufficient for invasion. Firstly, capillary forces may act to retard invasion of gas or other immiscible fluids. Secondly, if the fluids are considered to have a yield stress (which the cement slurry is), then invasion implies movement of the static fluids in the annulus and this means that the fluid must yield. It is natural to ask, what is the effect of immiscibility and yield stress on the invasion process? This is the topic of problem 2.

Problem 2 considers invasion of fluid into a tall column of stationary yield stress fluid (the cement slurry), through a single small hole. The single inlet mimics the isolated nature of a single pore. In hydrocarbon bearing rocks the permeability varies widely, from μm size pores in conventional oil reservoirs, down to the nm range for many tight or unconventional reservoirs, e.g. the Montney shale in Northeastern British Columbia. For porosity ranges $\leq$4%, the pores abutting the newly drilled borehole are essentially isolated holes on a surface, i.e. statistically. The flow considered in project 2 applies pressure to an invading fluid that can enter the column through a centrally positioned small hole in the lower surface of the container. The lower wall allows for symmetry in the apparatus and buoyancy should not be a factor on the pore scale before invasion has occurred.

This constitutes the industrial background to problem 2. The academic/scientific background is given in more detail in Zare et al (2016), Zare & Frigaard (2018a).

Problem 1: Micro-annulus formation during mud removal

In this problem we study displacement flow of a Bingham fluid (mud) by a Newtonian fluid (spacer/preflush/slurry) of different density, in the upwards direction along a vertical plane channel. All flows studied are laminar. We have studied both density stable displacements (spacer denser than mud; Zare et al (2017)) and density unstable displacements (mud denser than spacer; Zare & Frigaard (2018b))

Methodology

The methodology is computational and analytical. The first basic analysis is a dimensional analysis that reduces the parameter space to the following 4 dimensionless groups:

- Reynolds number: $Re = \rho U_0 D/\mu_1$
- Froude number: $Fr = U_0\sqrt{|At|gD}$, where $At = (\rho_1 - \rho_2)/(\rho_1 + \rho_2)$
- (Newtonian) Bingham number: $B_N = \tau_Y D/(\mu_1 U_0)$
- Viscosity ratio: $m = \mu_2/\mu_1$

The gap width of the channel is D, the mean velocity is U_0, $\rho = 0.5(\rho_1 + \rho_2)$ is the mean density, the viscosity of the displacing fluid 1 is μ_1, the yield stress and plastic viscosity of fluid 2 are τ_Y and μ_2, g is gravitational acceleration. The Reynolds number gives the ratio of inertial to viscous stresses, the Froude number measures inertial to buoyancy stresses, B_N measures the ratio of the yield stress to the viscous stresses in the displacing fluid.

The most detailed tool used is a two-dimensional (2D) transient computational simulation of the displacement flow using a mixed finite element/finite volume discretization method and using the augmented Lagrangian method for the yield stress fluid. The method is described fully in Zare et al (2017). This is our main numerical experiment that we use to explore the above parameter space. We do this in a systematic fashion, varying B_N and m. The latter are not taken to extreme values ($0.1 \leq m \leq 10$) as it is often observed that the main effects of viscosity difference do not need asymptotically small/large ratios. Re and Fr are chosen in such a way as to give a fixed number of values of $\chi^* = 2Re/Fr^2$ (which is signed positive or negative, depending on whether density stable (χ^*) or unstable (χ)), covering the range 0 to 500. The significance of χ^* is as a ratio of buoyant to viscous stresses.

In total we have run over 1000 simulations using the above 2D code. These are run on desktop style single processors, taking a number of days/weeks each to run, but we have access to multiple processors through the Compute Canada infrastructure. The long CPU times come from using the augmented Lagrangian method (which needs to converge iteratively at each timestep) and from needing a relatively long channel to ensure that the initial conditions do not have a significant influence on the established flow.

Due to the long computational times (given that to apply to an annular geometry we would need to use a 2D simulation at each azimuthal position), we have looked for a simpler model that can predict some of the important flow regimes and characteristic behaviours, but very rapidly. To this effect we have developed a symmetric two-layer model that: (a) resolves the momentum balance in axial direction; (b) uses this solution to provide input for a thin-film style model of the interface propagation. We refer to this model and its various analyses as the 1D model below.

Results and Data

We summarize the results of density stable and density unstable studies separately.

Density stable displacements

First to give an idea of simulations and how static wall layers emerge, an example result is given below in Figure 4; from Zare et al (2017). The drilling mud (red) is displaced by the spacer (blue) and the left panel shows time-spaced snapshots of the two fluids along a vertical plane channel with aspect ratio 30:1. We observe a beautifully parallel interface emerging, separating the 2 fluids and the wall layer.

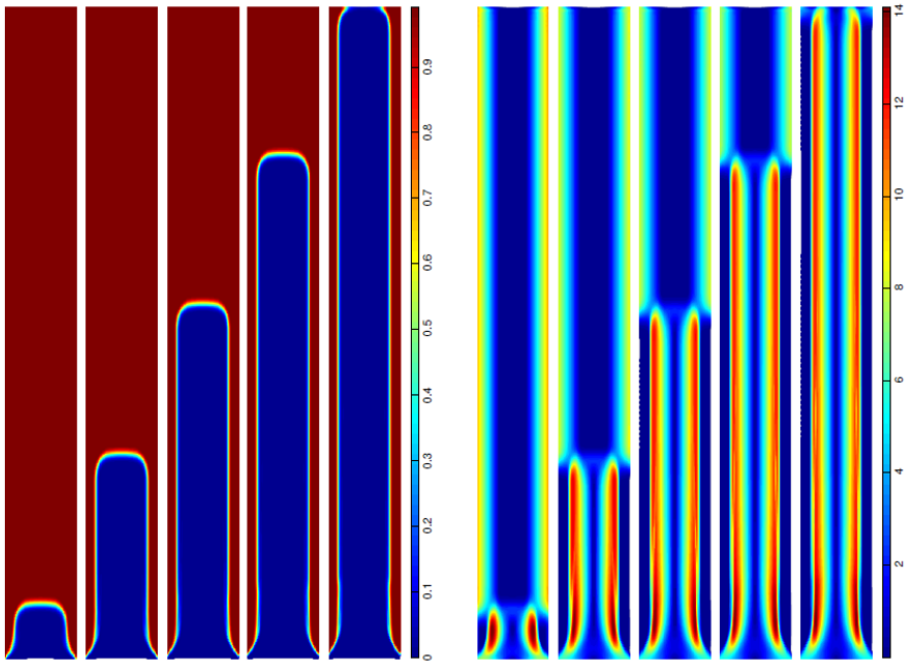

Figure 4: from Zare et al (2017). Example of a 2D displacement flow for $(Re, \chi^*, B_N, m) = (100, 200, 50, 10)$. ***Left: concentration profiles at successive times. Right: strain rate colourmaps at the same times.***

To get a feel for the parameters: $Re = 100$ suggests that the displacing fluid flow is inertial; $\chi^* = 200$ is a significant buoyancy force (as a comparison, the displacing fluid flowing on its own would require a (scaled) pressure gradient of 12 in order to flow at the same mean velocity, i.e. buoyancy is 17 times greater). The yield stress is 50 times greater than the viscous stress scale in the displacing fluid ($B_N = 50$), and the displaced fluid has plastic viscosity 10 times that of the displacing fluid.

The right hand panel shows the strain rate in the fluids at the same times as for the left panel. We observe three distinct regions where the strain rate is zero. First in the centre of the displacing fluid stream, due to symmetry. Second, ahead of the displacement front where the mud moves as an unyielded plug (common in all duct flows). Thirdly and most importantly, we observe the wall layers have zero strain rate and consequently are static, i.e. this is the fluid dynamic phenomena by which the micro-annulus is formed locally. The terminology “micro-annulus” is unfortunate as there is no requirement in these models that the wall layers occur all around the annulus. In any significantly eccentric annulus this would actually be unlikely: instead patches of wall layers are more likely. This contrasts with other micro-annuli, e.g. those due to shrinkage effects.

Figure 5 shows the maximal possible static wall layer thickness that can occur in a density stable displacement. The dimensionless layer thickness h below occurs on both walls of the channel, so that $2h$ represents the fraction of the channel that can have a static mud wall layer. There can be no static layers for $B_N < 6$, (the viscous stress of the displacing fluid alone exceeds the yield stress). We observe that the maximal layer thickness increases with B_N and that it decreases with χ^*.

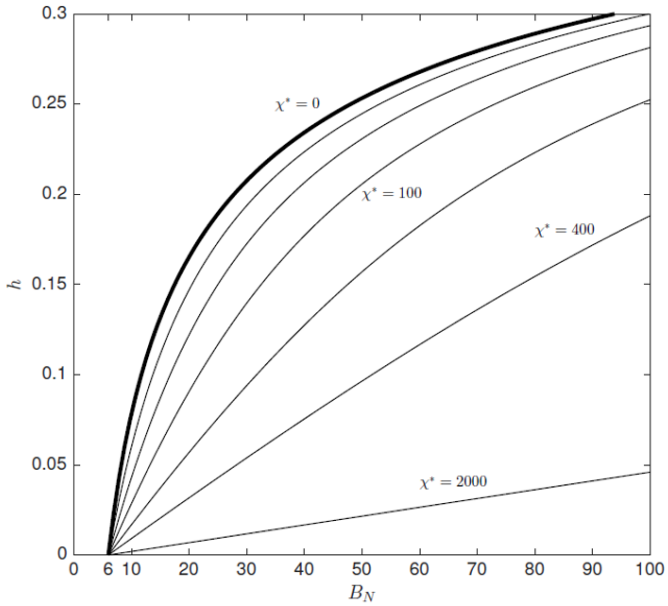

Figure 5: from Zare et al (2017), showing variations in h_{max} for $\chi^* = 0, 20, 50, 100, 200, 400, 2000$.

The maximal layer thickness is calculated from a 1D momentum balance. In practice the layer thickness actually found is selected by the dynamics of the displacement front and h_{max} just gives an upper limit for a static layer. The 1D analysis can also have a static layer h that is thinner than h_{max}. Equally, a 2D simulation could produce a layer that is thicker (at a given instance in time), but is not fully static or perhaps not fully 1D.

Figure 6 shows the mean layer thickness actually computed in the 2D simulation. These are averaged over the last part of the channel as the front has left the channel. The flows are established/developed, but could still be transient in time if the layer happens to still be mobile. The layers have been plotted against $(m + B_N)$, which is a measure of the effective viscosity in the displaced fluid. Subfigures a & b are at fixed buoyancy with increasing inertia (Re), which does not appear to have a significant effect on layer thickness. Subfigure c shows the effects of a significant increase in buoyancy χ^*, which appears to greatly thin the residual layer thickness.

In each plot we have h increasing with viscosity ratio m, which is intuitive. As each series of markers is at fixed , the x-axis effectively shows the effect of increasing B_N . Surprisingly the effect is not to increase the layer thickness, but rather we see a mild reduction in layer thickness with B_N may appear paradoxical. This reduction has been observed before in iso-dense displacements by Allouche et al (2000) and it is notable that here it occurs at a modest buoyancy χ^*. In the last subfigure we see that for large buoyancy χ^* there is in fact a slight increase in h with B_N. The cause of these counterintuitive layer thickness variations is in fact related to the dynamics of the displacement front. Figure 7 (left) shows a Newtonian displacement flow and the right panel shows the same but with B_N=50.

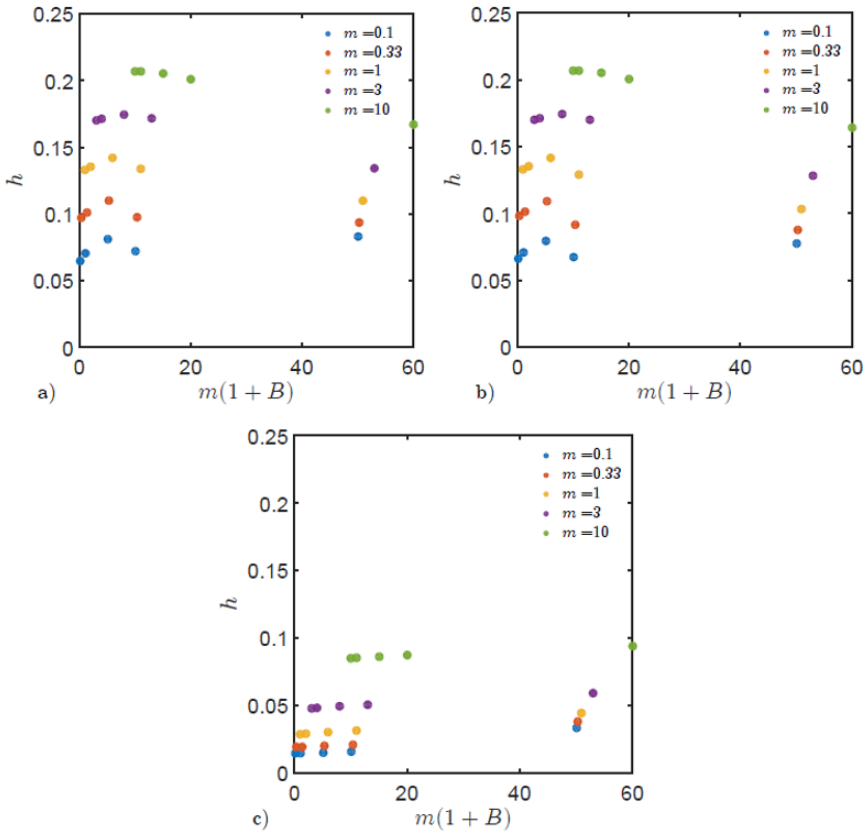

Figure 6: from Zare et al (2017). Thickness of residual layer h from the simulations, plotted against an effective viscosity ratio: $m + B_N = m(1 + B)$*, with: a)* $(\chi^*, Re) = (20, 0.1)$*, b)* $(\chi^*, Re) = (20, 20)$*, c)* $(\chi^*, Re) = (1000, 5)$*.*

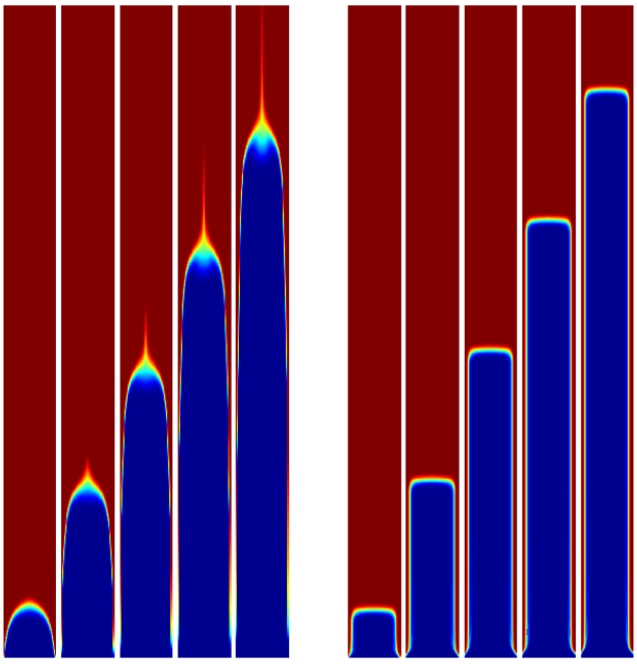

Figure 7: from Zare et al (2017): 2D displacement. Displaced fluid is red and displacing fluid is blue: a) $(Re, \chi^*, B_N, m) = (0.1, 20, 0, 0.1)$*; b)* $(Re, \chi^*, B_N, m) = (0.1, 20, 50, 0.1)$*. Approximate time of simulations:* $t = 2, 7, 12, 17, 22$*.*

As we see, the larger B_N produces a flatter displacement front (and velocity profile). The left-hand profile disperses downstream whereas the right-hand side moves in a plug-like *shock* wave. This is mainly the effect we observe that leads to the strange decrease in layer thickness with increased yield stress. Note too that there is an underlying competition here, as we have seen that increasing yield stress increases the maximal static layer thickness. For the larger buoyancy we do not see the same effect: the interface profiles are flattened here by buoyancy and increasing B_N can give a thicker layer, as expected.

The computations in figures such as Figure 7 take a number of days to run on a single processor desktop machine. This makes them difficult to think of as a design/optimization tool. Thus, we have sought methods that might predict the long-time behavior of these simulations without having to make an expensive computation. To this end we have analyzed our results in the following ways.

- We have characterized the behavior of the displacement front: firstly extracting a front velocity V_f from the numerical solutions; secondly we have categorized the front behavior as either frontal shock, spike or dispersive.
- For each simulation we computed the wall layer thickness h, by averaging the flow in the last part of the channel.
- For each parameter set we have also computed h_{max}
- We developed a 1D lubrication/thin film model of the displacement flow

If the flow has $h_{max} = 0$, then we have no risk of a micro-annulus. For $h_{max} > 0$, we compare if $h > h_{max}$ or $h < h_{max}$. In the former case the layer should be mobile, but at long times we will have $h \to h_{max}$ as the layer slowly thins. On the other hand if $h < h_{max}$, then the layer is static. From the computed front velocity V_f (or shock velocity, V_s) we have a layer thickness h_f (or h_s) to conserve mass, i.e. $h_f = 0{,}5\left(1 - 1/V_f\right)$. We find that there is a near-perfect match between the frontal classification and whether or not $h > h_{max}$, i.e. $h < h_{max}$ is a frontal shock and $h > h_{max}$ is a spike; see Figure 8.

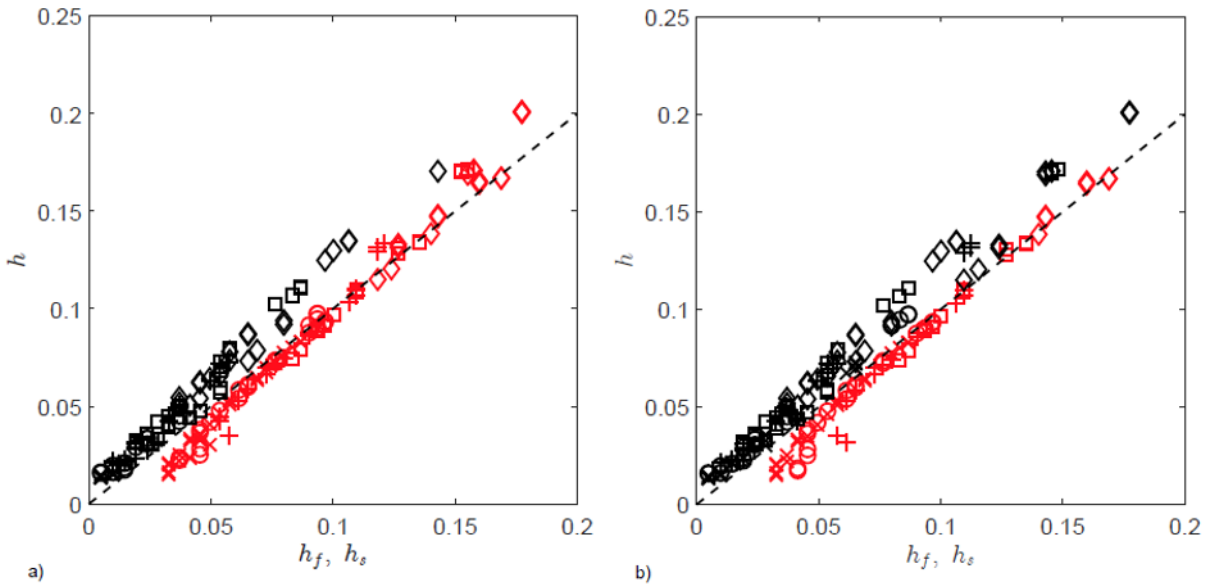

Figure 8: Classification of computed h, for $h_{max} > 0$: a) frontal shock (red), spike (black); b) $h \leq h_{max}$ (red), $h > h_{max}$ (black). The symbol shapes denote different values of m: see Figure 19 in Zare et al (2017).

Next we considered the 1D lubrication/thin film model of the displacement flow. Just as with the 2D simulations, these displacement flows soon converge to a steady (long-time) motion, which can also be classified as either having a contact shock, a spike or being dispersive. In general, the interface motion in the 1D model is faster than that in the 2D model, perhaps because components of the stress tensor are neglected. This aspect of the 1D model

was therefore not found to be useful. However, the front classifications were found to be in good agreement with those of the 2D model (see Figure 9).

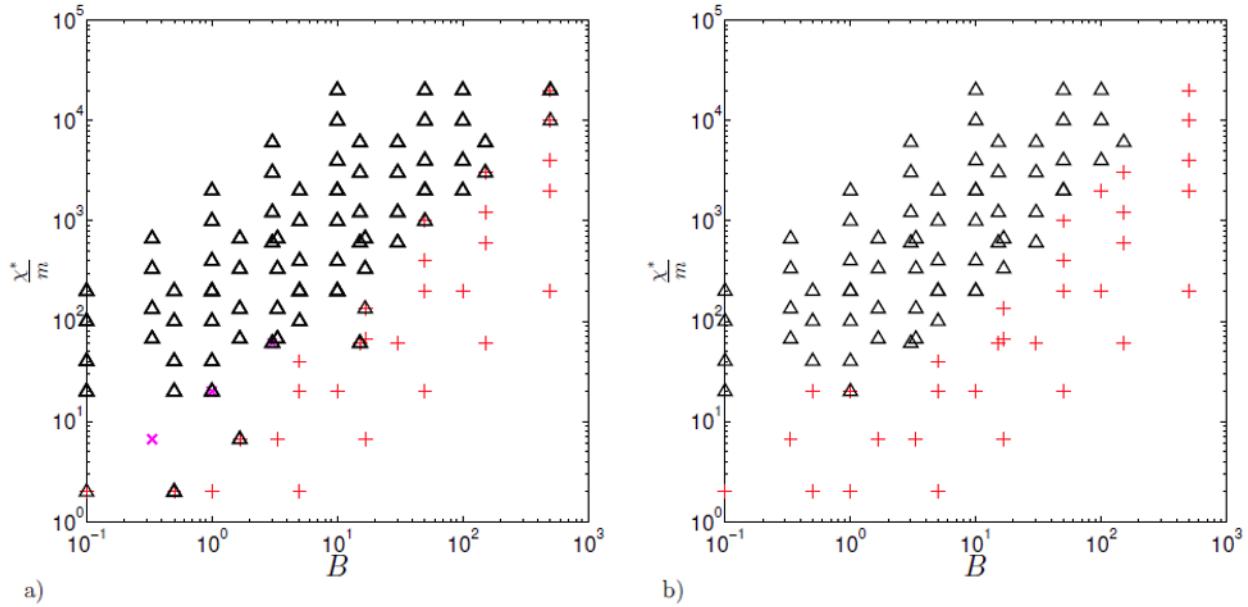

Figure 9: Displacement flow classification: a) 2D computations; b) thin film/lubrication model rom Zare et al (2017). Symbols: spike = triangle, frontal shock = +, dispersive = x.

Computation of the 1D flow is significantly quicker than that of the 2D flow. One can also analyze the 1D model without ever having to calculate the actual interface motion. This is even faster. Equally, the calculation of maximal static layer thickness is very fast. Thus, we can determine quickly whether:

- $h_{max} = 0$
- $h_{max} > 0$, and at long times $h \to h_{max}$
- $h_{max} > 0$, and $h < h_{max}$ (but h remains unknown)

In the last 2 cases we have a static wall layer and we can at least compare h_{max} to optimize this feature of a design.

Density unstable displacements

Density unstable displacements have been studied with the same methodology, computational and analytical tools as the density stable flows outlined above. Conceptually, these would be lightweight spacers or washes – although for the latter note that our flows are laminar. The results we summarize here are taken from Zare & Frigaard (2018b).

The first major change compared to the density stable displacements was that many of the flows showed instabilities. Although for $\chi < 10$, the flows were broadly similar to the density stable flows with small χ^*, as the buoyancy parameter χ grew instabilities commenced. An example stable flow is shown in Figure 10 (top left).

Many flows would destabilize at the front in a form of Rayleigh-Taylor (RT) instability (Figure 10, top right). Most however, had a stable symmetric front and initially apparently uniform stable parallel wall layers along the sides of the advancing finger. However, these parallel layers then destabilized in many cases. For smaller values of m the instability took the form of a wave-like disturbance and appeared to be related to the different velocities of the two layers (Figure 10, bottom). These flow features are characteristic of Kelvin-Helmholtz (KH) waves. Although the instability mechanism is inviscid we have to recognize that viscosity plays a significant role in determining the type of

parallel flow. More explicitly, for $m < 1$ the displaced fluid plastic viscosity is small and this means that it is easier for a counter-current flow to develop (i.e. a backflow).

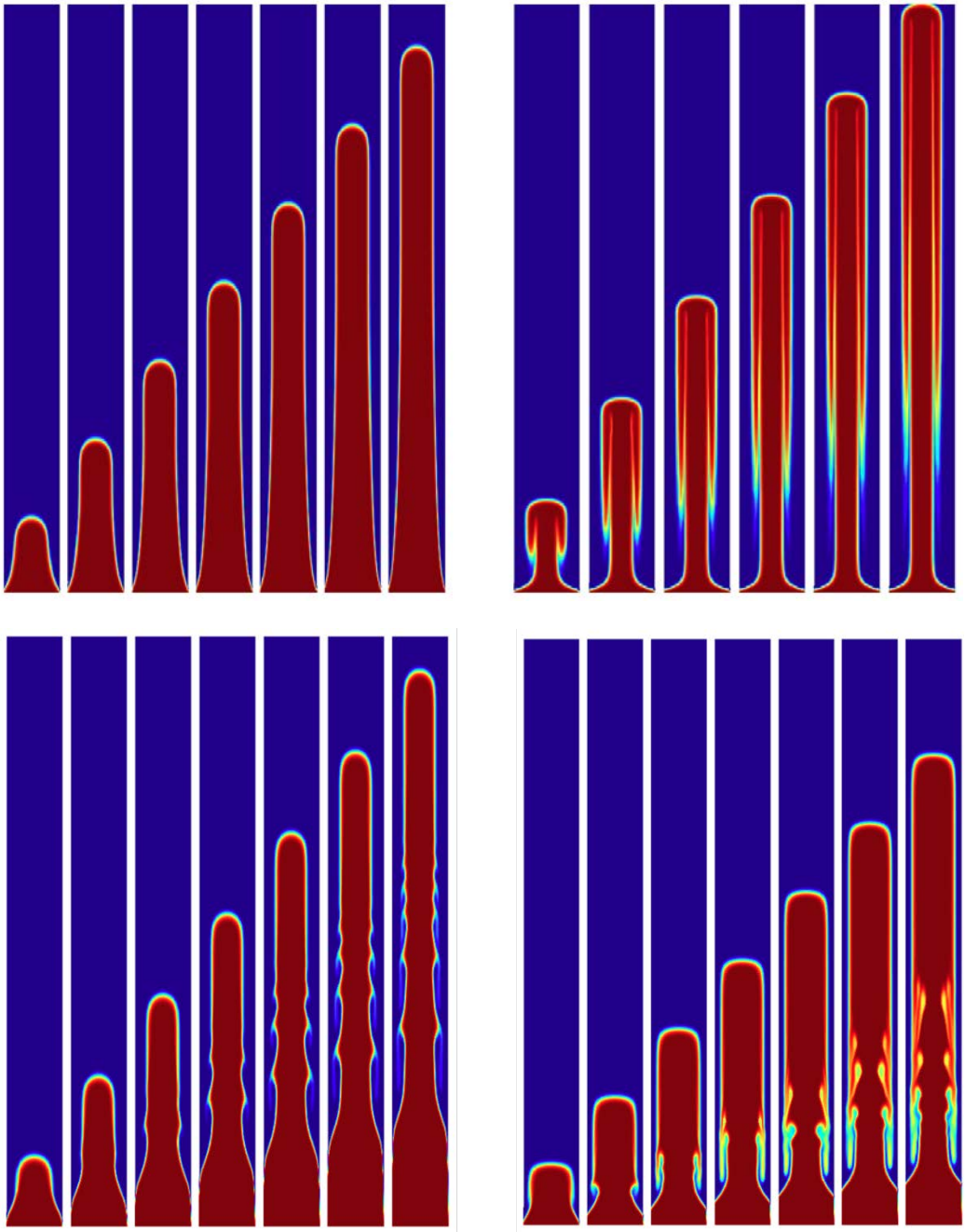

Figure 10: Example displacement flows: $(Re, \chi, B_N, m) = (15, 10, 5, 10), (25, 500, 5, 3), (50, 100, 1, 0.1), (25, 50, 0, 0.33)$*, (from L-R, Top-Bottom). Images from Zare & Frigaard (2018b).*

For larger viscosity ratios $m > 1$ the type of instability is different. We see initially inverse bamboo waves (i.e. like a bamboo profile, but the points are inwards) and sometimes an evolution into pearl/mushroom type structures; we classify these as IBM instabilities. These types of instability are related to one another and found in multi-layer flows with a more viscous fluid near the wall. IBM instabilities have been studied less intensively than KH instabilities. Although wave-like, they move and evolve slowly as they are controlled by the larger viscosity of the wall layer.

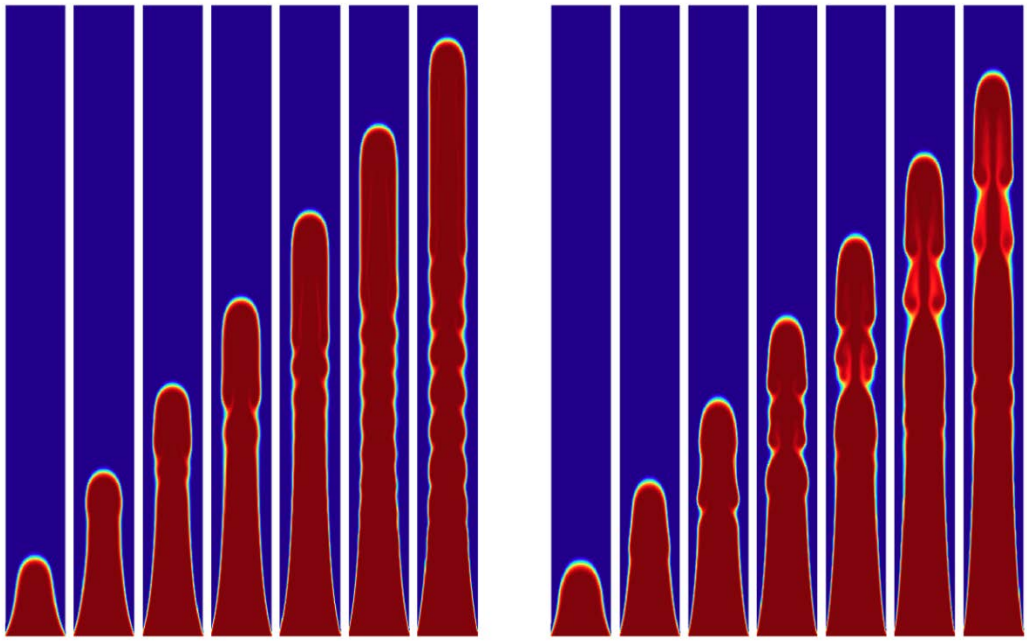

Figure 11: Example flows: $(Re, \chi, B_N, m) = (270, 180, 1, 10), (500, 100, 5, 10)$*, (from L-R). Images from Zare & Frigaard (2018b).*

To give an overview of where the different flow types are found we have created "panoramas" of the flows. In these we plot the flows against Re and χ, for different combinations of (B_N, m), at the same time classifying as either stable or unstable and RT, KH or IBM. These are shown in Figures 12 and 13 below. We can see that the RT instability may occur with either KH or IBM, or even for a stable flow. We also see that many flows in the regimes shown are stable and that stability increases with B_N, as might be expected.

Our data range extends outside that shown in Figures 12 and 13, but these show the transitions that are induced by either increasing inertia (Re) or buoyancy (χ), at fixed viscosity. Within these ranges, increasing B_N above 5 has little effects as the flows are largely stable. Although useful as a visual tool, Figures 12 and 13 are less useful in terms of understanding quantitatively where the flows change. For this we have plotted the flow regimes against Fr and Re/Fr (see Figures 14 and 15). The former measures inertial and buoyant stresses. The ratio Re/Fr balances buoyancy driven motion against the ability of the viscosity to dissipate the energy of that motion.

The transition shown in Figures 14 and 15 is marked with a broken line. This is really intended as a guide to the eye and is not a *curve fit*. What we see is that for small m the transition is simply a critical value of χ, i.e. the KH mechanism is triggered by the parallel flow structure which is wholly dependent on χ for fixed rheologies. However, the larger values of m lead to a transition that depends on a balance between Re and Fr, of the form $Re \propto Fr^k$ where k decreases with m, i.e. $k = 2$ at small m, decreasing to $k = 0.8$ at $m = 3$, and then $k = 0.4$, for $m = 10$.

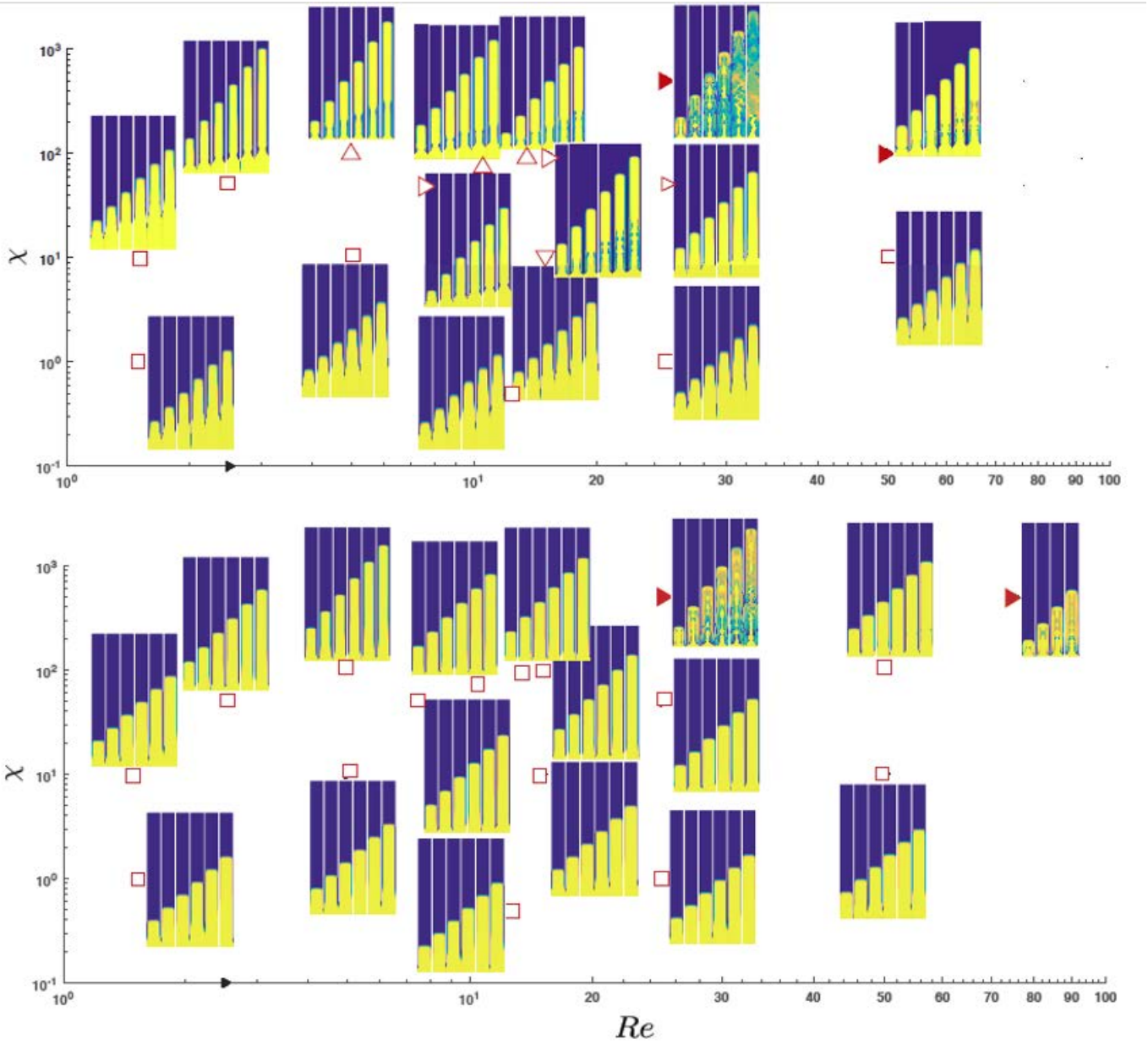

Figure 12: From Zare & Frigaard (2018b). Panorama of flow types for $m = 0.1$ and $B_N = 1$ (top), $B_N = 5$ (bottom). For $B_N = 10$ the flows are similar to $B_N = 5$. The markers indicate the data position in the (Re, χ)-plane and the flow classification: square – stable; triangle – KH; circle – IBM; filled symbols – RT.

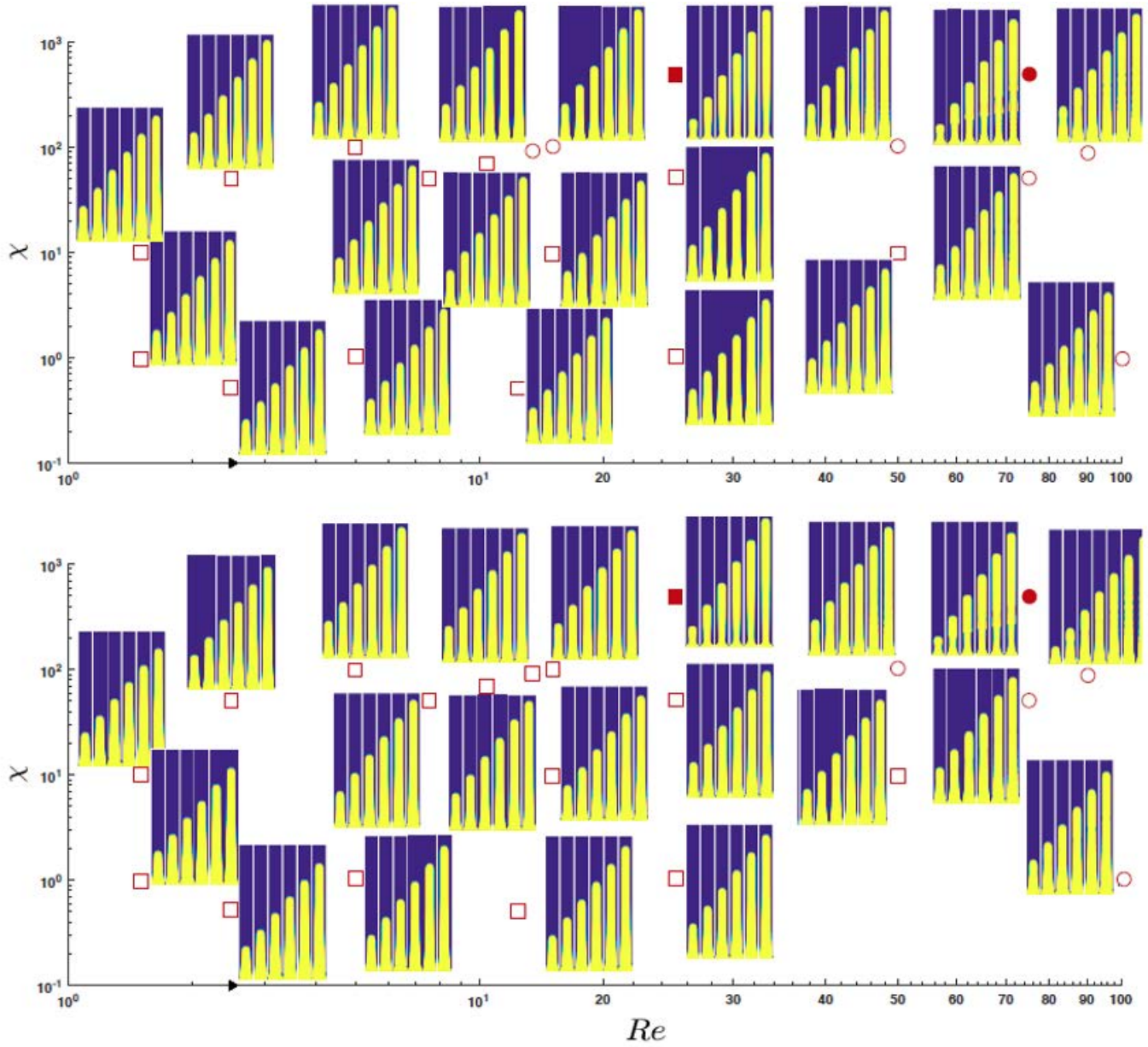

Figure 13: From Zare & Frigaard (2018b). Panorama of flow types for $m = 10$ and $B_N = 1$ (top), $B_N = 5$ (bottom). For $B_N = 10$ the flows are similar to $B_N = 5$. The markers indicate the data position in the (Re, χ)-plane and the flow classification: square – stable; triangle – KH; circle – IBM; filled symbols – RT.

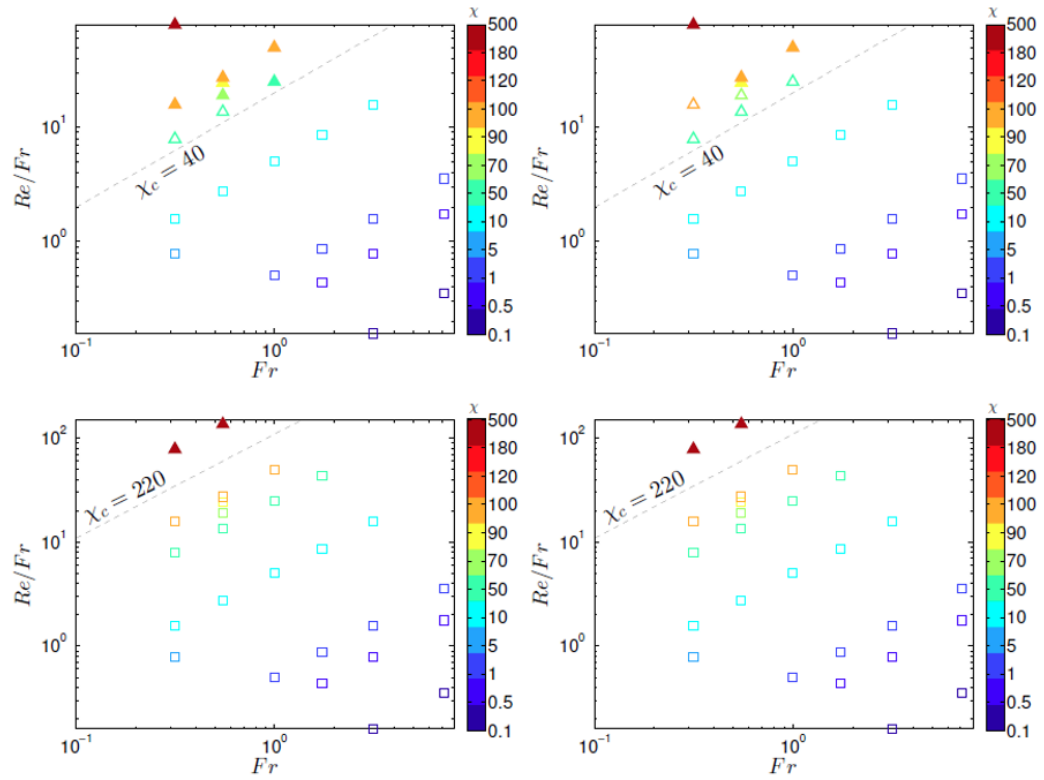

Figure 14: From Zare & Frigaard (2018b). Stable and unstable parameter regimes for $m = 0.1$ and: a) $B_N = 0$; b) $B_N = 1$; c) $B_N = 5$; d) $B_N = 10$. The markers indicate flow classification: square – stable; triangle – KH; circle – IBM; filled symbols – RT.

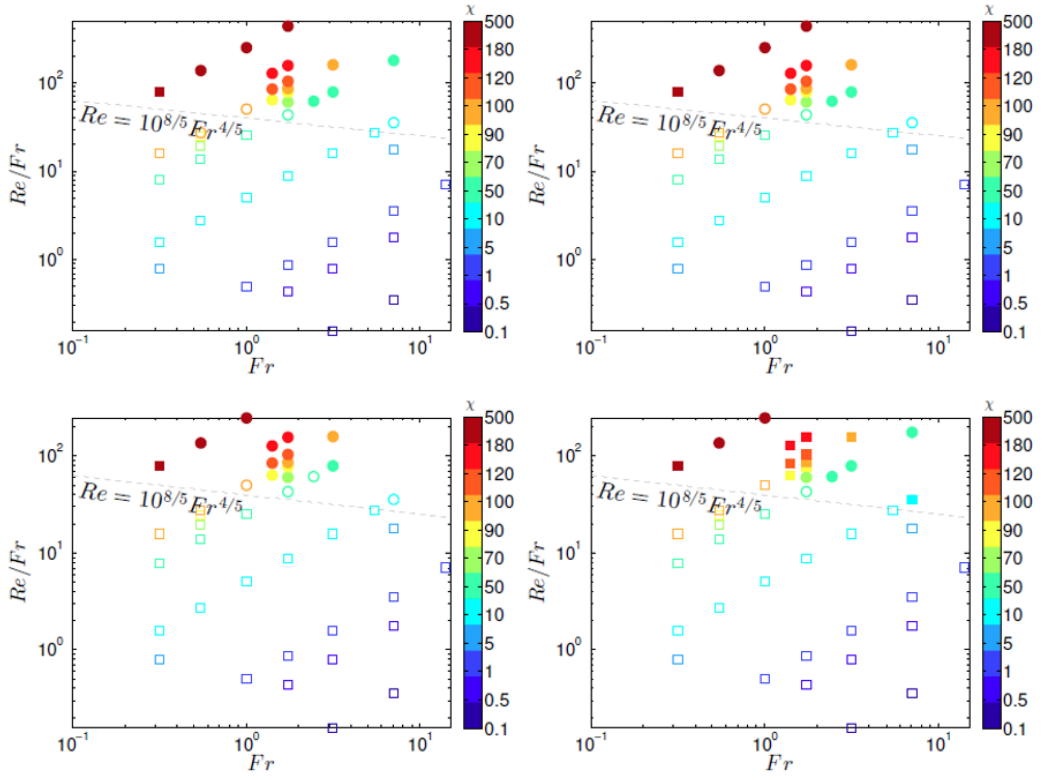

Figure 15: From Zare & Frigaard (2018b). Stable and unstable parameter regimes for $m = 3$ and: a) $B_N = 0$; b) $B_N = 1$; c) $B_N = 5$; d) $B_N = 10$. The markers indicate flow classification: square – stable; triangle – KH; circle – IBM; filled symbols – RT.

The next stage of our study has looked at the all important phenomenon of static wall layers for density unstable flows. The first analysis simply tried to extend the idea of a maximal static layer from the density stable flows in Zare et al (2017). This worked well for small enough $\chi, (< 10)$, for which the buoyancy forces are less than the pressure gradient forcing the flow; see Figure 16a. However, as χ becomes larger the problem becomes more complex. If we insist that the entire wall layer is static, then we are able to compute the pressure gradient and calculate precisely the stresses in both layers. We observe that as χ increases, the stress gradient in the static layer switches from negative to positive. We are able to delineate the regimes where the wall shear stress changes sign and where the shear stress is maximal at either the wall or the interface. These 4 regimes are shown in Figure 16b. Fixing χ and varying the interface position, we can plot the maximal shear stress generated in the wall layer (see Figure 16c), which we find to be monotone provided that we do not enter into regime 4, where the wall shear stress is maximal and positive. For such values of χ it appears that a maximal static layer thickness would not be continuously defined. For the other values of χ we were able to define a new $h_{max,a}$ that denotes the maximal layer thickness where the entire layer is static; see Figure 16d.

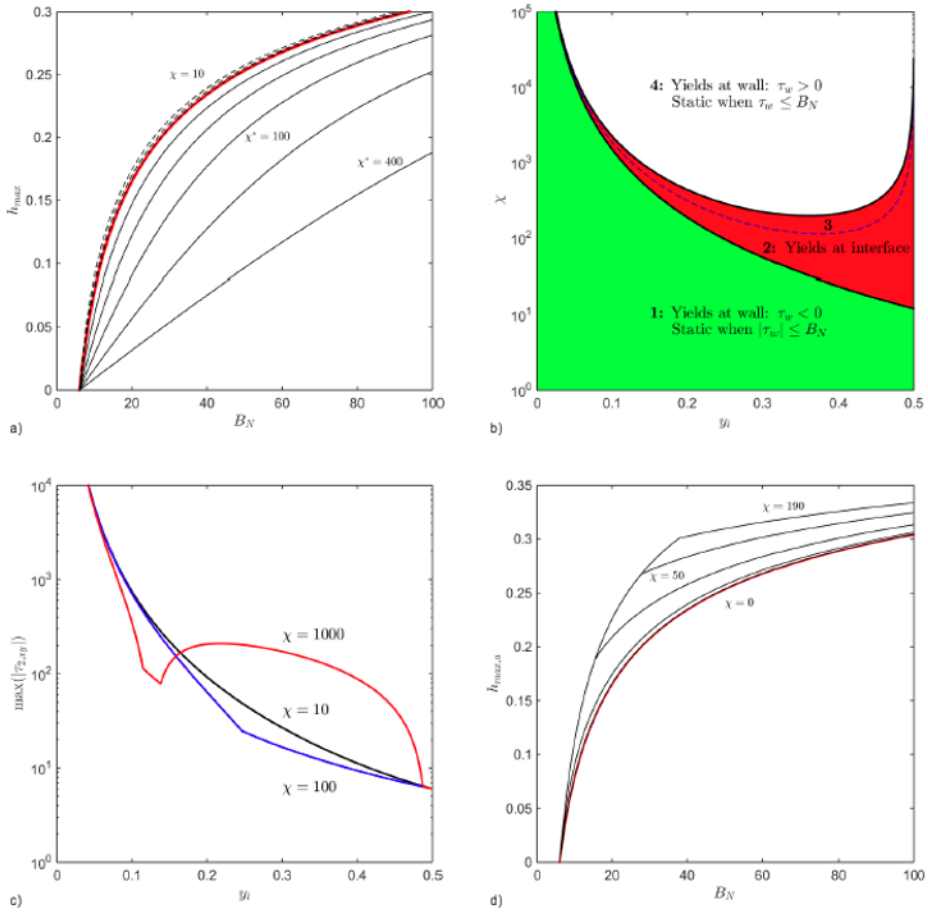

Figure 16: a) Plot of h_{max} using the definitions from Zare et al (2017), extending to $\chi < 12$. b) Location of regimes 1-4 in the (y_i, χ)-plane. c) Variation of the maximal shear stress in the wall layer, plotted for $\chi = 10, 100, 1000$. d) Plot of $h_{max,a}$ for $\chi = 0, 10, 50, 120, 190$.

The occurrence of the transition between regimes 2 & 3 in Figure 16b suggested that: (a) the wall layer would yield first at the interface and not the wall; (b) as the layer yields, the sheared fluid will be pulled upwards along the channel, but could leave behind a partially static wall layer. We checked if this did happen in our numerical solutions and found that it did indeed occur frequently (see Figure 17). Furthermore, some 1D calculations revealed that the

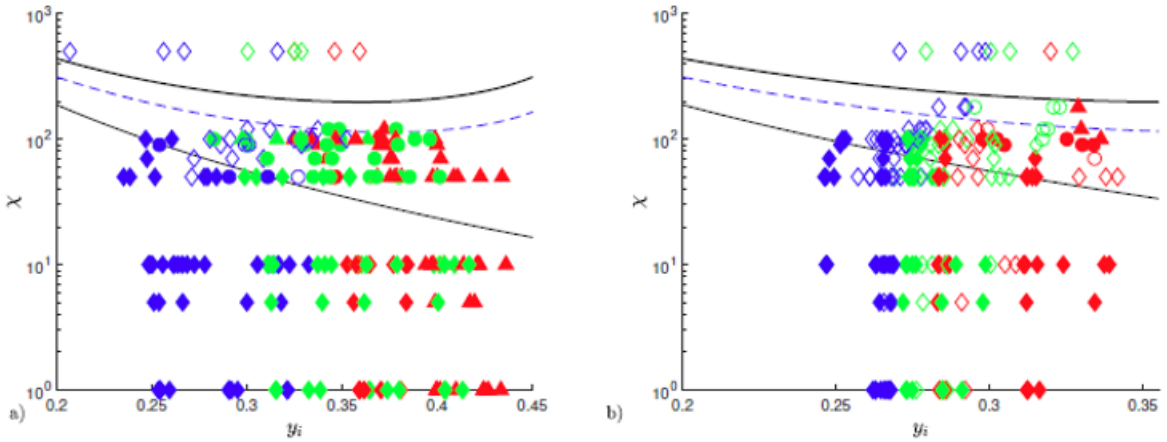

Figure 17: Values of interface position y_i as computed form the 2D simulations in Zare & Frigaard (2018b): a) $m \leq 1$; b) $m > 1$. The triangles, circles and diamonds are respectively: fully static, partially stati and moving wall layers; $B_N = 1, 5, 10$ are blue, green and red, respectively. The filled symbols are stable and empty symbols unstable. The lines represent transitions between regimes 1-4, according to the fully static analysis.

thickness of the static layer, when partially yielded, could in fact be larger than when fully static! Therefore, to compute the actual maximal static layer we need to consider also partially yielded wall layers. This new maximal static wall layer was denoted $h_{max,p}$ and it was found that $h_{max,p} \geq h_{max,a}$. We then classified our 2D computations as having either fully static, partially static or transient wall layers and were able to compare h with $h_{max,p}$. This revealed that all fully static and partially static layers were less than $h_{max,p}$ (within mesh tolerance), whereas the transient layers were often larger (Figure 18). Also significant in our results was to have partially static layers for $B_N < 6$, unlike for density stable flows, i.e. density unstable allows micro-annuli at smaller yield stress.

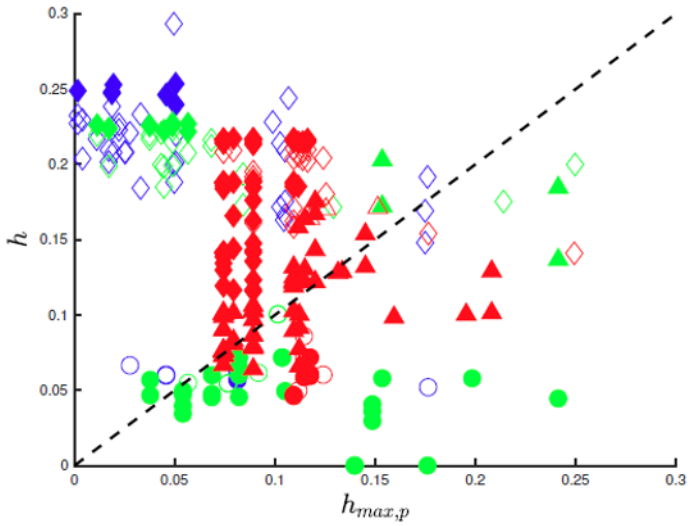

Figure 18: From Zare & Frigaard (2018b). Plot of h against $h_{max,p}$. The triangles, circles and diamonds are respectively: fully static, partially static and moving wall layers; $B_N = 1, 5, 10$ are blue, green and red, respectively. The filled symbols are stable and empty symbols unstable.

Two final analyses were conducted, to parallel what we did for the density stable displacements. First we extended the 1D thin film model from the density stable study of Zare et al (2017), classifying the front behavior in the same way, i.e. as frontal shock, dispersive, spike etc… There were also additional regimes with 2 shocks that moved at different speeds and sometimes counter-currently. Secondly, we compared the frontal classification with the previous classification of our 2D flows. We discovered that dispersive and frontal shock regimes matched very well with the classification of stable flows. Thus, again we are able to predict flow type reasonably well without the need for full 2D computation; see Figure 19.

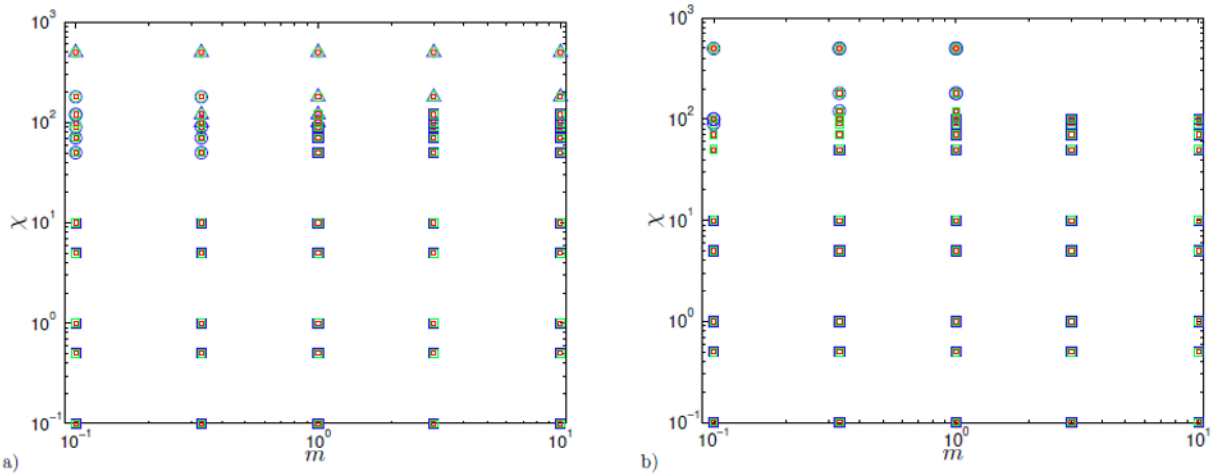

Figure 19: From Zare & Frigaard (2018b).a) Flow regime from the 1D thin-film model of Zare et al (2017): square – dispersive or only a single frontal shock; triangle – two shocks, leading and trailing; circle – the channel plugs up and displaces with shock speed unity. b) flow regimes classified in the 2D model: square – stable; circle – KH. In both figures $B_N = 1, 5, 10$ are blue, green and red, respectively and the marker size is chosen to decrease with B_N.

Discussion & Conclusions

Project 1 has given an in depth study of the fluid mechanical phenomenon of a wet micro-annulus. As commented earlier, to consider a full study of an annular displacement in this context would require mapping out a 12-dimensional parameter space. Through the various approximations outlined, this has been reduced to 4 parameters that still capture the main changes that one could consider at different points in a vertical annular displacement.

This study has explored both density stable and unstable displacements of a Bingham fluid by a Newtonian fluid along a vertical channel, over a broad range of viscosity ratios, Bingham, Froude and Reynolds numbers, with the latter 2 parameters selected to provide different values of $2Re/Fr^2$, which is the key parameter that defines a parallel multi-layer flow of the two fluids, balancing buoyancy and viscous stresses. In total, more than 1000 2D displacement simulations have been performed and analyzed. The main objectives have been to understand and predict residual wall layer thicknesses that result and the effects of the different parameters on displacement. The residual layers, when static, are the underlying mechanical embodiment of a (wet) micro-annulus as formed in primary cementing. Longer term micro-annulus formation, e.g. via shrinkage, is not considered.

For the density stable displacements, many of the parametric effects we have observed are intuitive: increasing m increases h and increasing χ^* decreases h. Thus as expected, increasing buoyancy or the displacing fluid viscosity

improves the displacement. Counter-intuitive however, is the decrease in h for increasing $B = B_N/m$, meaning the plasticity of the displaced fluid. This effect is most evident at small to moderate buoyancy: for large buoyancy the residual layers are anyway diminished. The effect also occurs in density unstable displacements, provided the buoyancy is small. A summary of our results in this respect is given in Figure 12 of Zare et al (2017), which shows that h is described very well as a function only of $(B_N/m, \chi^*/m)$.

The residual wall layer thickness h is measured near the end of our 2D channel simulations. As well as the size, a critical feature is whether or not the wall layer is moving. This depends on h and h_{max}, the maximal static wall layer thickness, which is easily computed and we find that $h_{max} = h_{max}(B_N, \chi^*)$; see Figure 5. If $h_{max} = 0$, (which occurs for $B_N \leq 6$) the wall layer is moving and will eventually be removed. If instead $h_{max} > 0$ we have 2 possibilities: either $h < h_{max}$ and the wall layers are static, or $h \geq h_{max}$ and the wall layers are moving. If the wall layers are moving and $h \geq h_{max}$, it follows that h will decrease and approach h_{max} at which point it becomes static.

The second part of the results on stable displacements has focused at prediction of the residual layer behaviour by classifying the displacement front behaviours. Our displacement flows have shown 3 characteristic behaviours: frontal shock, spike and dispersive. The first interesting result from examining our data is that when $h_{max} > 0$, we have only observed frontal shocks and spikes. Secondly, we have shown that frontal shocks appear to correspond to $h < h_{max}$, and spikes correspond to $h(t) \geq h_{max}$. This led to the interesting possibility of qualitatively predicting the residual layer behaviour from a simplified model (as opposed to carrying out a full 2D displacement). To this end we developed a lubrication/thin-film approach and have demonstrated that flow classification from the lubrication model is able to distinguish/predict the 2D displacement type, in terms of the frontal behaviour, and consequently the residual layer behaviour.

The observed characteristic behaviours of the displacement front are common to many other displacement flows. In Newtonian-Newtonian displacements, the wall layers are not strictly uniform as they thin during drainage, but are often approximated as constant thickness. Spike-type miscible displacements in Newtonian-Newtonian flows were first observed by Petitjeans & Maxworthy (1996) and by Lajeunesse et al (1999). The change from frontal shock to spike type flow is related to a transition in the streamline pattern, measured in a frame of reference at the shock speed; see Petitjeans & Maxworthy (1996). Here we have a diffuse interface and an imprecise calculation of the shock and frontal speeds from our numerical simulations, so that working in a moving frame is not a good diagnostic method for analyzing our 2D simulations. This type of computation has been performed effectively by Freitas et al. (2011,2013) using an interface-fitted mesh, considering both immiscible Newtonian and visco-plastic fluids.

Industrially we may adopt the following rubric for stable displacement configurations.

(i) Compute $h_{max}(B_N, \chi^*)$ if $B_N > 6$ (otherwise the displacement is effective: $h(t) \to 0$ as $t \to \infty$).

(ii) Analyze the flux function from the thin-film displacement model and use this to classify as either a spike or frontal shock.

(iii) If a frontal shock, expect to have a uniform static wall layer that forms during the displacement and will remain, with thickness $h < h_{max}$.

(iv) If a spike, locally expect an initially moving wall layer, following passage of the displacement front, and eventually $h(t) \to h_{max}$ as $t \to \infty$.

Thus, only 3 long time behaviours occur: $h(\infty) = 0,\ h(\infty) = h_{max}$ or $h(\infty) < h_{max}$ (frontal shock). Although lacking the precise layer thickness in the frontal shock case, $h(\infty)$ is bounded and the above steps require only very quick calculations, i.e. solution of algebraic equations, which could be embedded in a process design/optimization calculation.

In considering how one might improve this (i.e. in the case of frontal shocks, with $h(\infty) < h_{max}$), the first option is of course 2D computation, either as here or using a front-fixing method such as Soares et al (2009) or Freitas et al (2011) (at large Capillary number). Although the computations of Soares et al (2009) and Freitas et al (2011) are attractive and are probably quicker than the transient computations here, they are restricted to $Re = 0$, and proceed by assuming a steady state configuration. In particular, some of the recirculatory patterns predicted in these studies are not likely to be found in practice as the interface evolves away from the steady state, e.g. the formation of spikes occurs as explained in Petitjeans & Maxworthy (1996). In an idealistic laboratory setup, one could do reasonably well without computation. Following the type of analysis in Soares et al (2009), if one monitored the total pressure drop and flow rate as the displacement progressed, it would be possible to predict the pressure gradient from the multi-layer flow region and hence compute interface position. This however requires differentiating the pressure drop with respect to time, which can be problematic in noisy industrial settings with limited data, such as primary cementing.

In the primary cementing context, although the rubric presented above for stable displacements is a significant advance in our ability to predict micro-annulus formation, it leaves the question of what is best? Dispersive or spike type displacements result in moving residual layers. The timescale for these layers to be removed will increase with m (potentially also with B_N/m) and these mobile layers should be regarded as potential sources of contamination during the cement placement. We have seen no evidence of instability in our simulations, but these are of limited duration. The velocity profiles in these draining wall layers have pseudo-plugs at the interface, i.e. yielded at the wall only but with a plug velocity that would slowly vary along the channel (annulus). Visco-plastic lubrication studies would suggest stability (e.g. Moyers-Gonzalez et al, 2004) but viscous-viscous theories (e.g. as summarized in Joseph & Renardy, 1993) often show instability when the more viscous fluid abuts the wall. On the other hand, the frontal shocks, produce a static layer $h(\infty) < h_{max}$ as soon as the front passes. These mud wall layers will be hydrodynamically stable and remain. There is no contamination risk from interfacial mixing, but such layers are likely to dry during cement hydration, forming a porous conduit. In this context, the spike displacements at large $m$appear to be the worst case: not only do we suffer the contamination risk of mobile layers over a timescale $\propto m$, but also the layers at best thin and approach $h(\infty) \sim h_{max} > 0$, and remain on the walls.

For density unstable displacements (Zare & Frigaard 2018b) of a Bingham fluid with a Newtonian fluid, the overall picture of displacement flows is more complex than for the density stable configurations. First, although there are many stable displacements that are qualitatively similar to the density stable flows, we also observe 3 broad categories of instabilities: frontal instabilities of Rayleigh-Taylor (RT) type, interfacial roll-waves of Kelvin-Helmholz (KH) type and viscous-controlled inverse bamboo and mushroom (IBM) morphologies. Each instability classification is interpreted loosely as in practice other physical effects are present and displacement flows are not idealised for the study of individual instabilities.

In general, increasing the buoyancy χ when the displaced Bingham fluid is less viscous than the displacing fluid leads towards a counter-current flow and KH instabilities are observed in this scenario. This tends to be a combination of low m, weak B_N and strong χ. IBM instabilities are generated when $m > 1$ and a two-layer structure is initially formed. Since $m > 1$, they have a slow growth rate controlled by the viscosity of the displaced fluid. Within the IBM classification we have also observed an interesting regular patterning of static wall layers (*footprinting*); discussed further in Zare & Frigaard (2018b)

The transition between stable and unstable regimes has been plotted in the $(Fr, Re/Fr)$-plane. It happens across a boundary of form: $Re \sim Fr^x$, where x is 2, 8/5, 4/5, 2/5 depending on m and B_N. The exponenent x decreases with increasing m values and slightly increases with B_N. Our study has been phenomenological in this aspect, so these transitions are intended more as a guide rather than as any serious attempt to curve-fit data. In terms of these parameters, although Re/Fr is useful to plot against, it is worth noting that this balance does not represent the viscosity of the displacing fluid at all: including m and B_N would be a potential improvement.

We have also explored static residual layers for density unstable flows. First, by assuming that fluid 2 is completely static, four flow regimes have been identified in our two layer model: 1- τ_{xy} decreases from zero in the center toward the wall, and the maximum absolute value will occur at the wall; 2- by increasing χ further the slope of τ_{xy} is reduced in layer 2, but still the interfacial and wall shear stress are negative; 3- by increasing χ further the wall shear stress becomes positive, but is still smaller than the interfacial stress; 4- the wall shear stress is positive and bigger than the negative interfacial stress.

The above classification was based purely on the stress distributions τ_{xy}. The fluid 2 layer next to the wall can be static or moving in all regimes, depending on B_N. However, the interesting fact is that the wall layer can be partially yielded in regimes 2 & 3, such that a layer near the interface yields and is moved in the flow direction, but the wall layer remains static. For regimes 1-3 we have extended the concept of the maximal static wall layer to define $h_{max,a}$, where all of the fluid 2 layer is static. However, it is apparent that when the wall layer yields in regimes 2 or 3, there will be a partially static layer and potentially the partially static layer could be thicker than the fully static. This is because, by yielding and moving slightly the fluid 2 layer contributed to the flow rate, hence reducing the pressure gradient and shear stresses.

The residual layer left on the wall in our 2D simulations was analysed, using a similar method as for the density stable displacement, but now also averaging the wall and interfacial stresses. This layer can be: 1- fully static; 2- partially static; 3- fully moving. We have seen that fully moving layers can happen at all χ, m and B_N values whereas partially static layers lie in regimes 2 & 3, as predicted by a 1D parallel layer model. For $m \leq 1$, fully static layers for $B_N = 10$ can develop in regimes 1, 2 and 3 but for $m > 1$ they are distributed only in regime 2 & 3. For $B_N \leq 6$, all the layers are moving or partially static except a few fully static layers which are very close to the yielding threshold, i.e. within numerical error. Similar to the results obtained for stable displacements, the thickness of residual layer increases with m and decreases with B_N.

As well as our stress-based analysis, we have solved the 2-layer model computationally, so that the stress profiles are now those actually found as part of the velocity (and pressure gradient) solution, and not simply inferred from the momentum balances and constraint of a static wall layer. Using this, it is observed that at any given set of (B_N, χ, m), the yield surface position y_Y varies with interface position y_i over a U-shaped curve which either has a single minimum or is discontinuous with the middle part broken. This structure leads to the simple calculation of the minimal y_Y and hence a new maximal static layer $h_{max,p}$. The maximal static layer $h_{max,p} \geq h_{max,a}$, and accounts for partially static wall layers.

The industrially important results are that: (i) partially static wall layers can be formed for $B_N < 6$, unlike for the density stable case; (ii) the partially static wall layers can for certain parameters yield a layer thickness larger than for a fully static wall layer; (iii) in agreement with 1D-model results, the thickness of wall layers obtained from 2D-computations in fully static regime are mostly less than $h_{max,p}$. A few cases have slightly thicker layers which may be due to the numerical procedure.

Finally we have explored a thin-layer version of the 2-layer 1D model, as was done for the density stable case. Also here the displacement front predictions from the 1D model are predictive of behaviour on the 2D simulations. Here we are able to predict stable flows and those susceptible to KH type instabilities. One of the questions we had in starting this research direction in particular, was whether instabilities induced by the fluid rheology differences could act to destabilize the wall layers, resulting in thinner wall layers. Considering the range of our results, we don't see any evidence of this, although on the timescale of the well annulus it must be admitted that our results only reflect a very local and shorter time displacement.

In the above respect, we feel that density unstable flows do not have any positive effect on wall layers/wet micro-annuli, and probably the reverse. The $B_N < 6$ criterion for eliminating static wall layers in stable displacements is not valid for density unstable displacements and we must balance the (unproven) potential for destabilization with the demonstrated ability of having partially static residual layers as we increase χ.

In terms of future directions, both the density stable & unstable flows analyzed have a temporal aspect that is not well explored and is perhaps also relevant in the cementing context. Although cemented annuli are long they are not infinite. Also the bottom of the well sees a longer displacement time (e.g. measured from arrival of the first displacing fluid) than does the top of the cemented interval. We should also note that thin layers move (asymptotically) slowly in any model so the asymptotic behavior of the wall layer h, practically may not be attained at all points in the annulus.

These 2 papers complete the study of displacement flows of a yield stress fluids by a Newtonian fluid along a vertical channel. Iso-dense displacements were studied by Allouche et al (2000) and by Wielage & Frigaard (2011), which we have complemented with density stable displacement flows (Zare et al, 2017) and density unstable flows (Zare & Frigaard,2018b). Of course, the results are only complete in considering a Newtonian fluid displacing a Bingham fluid in a vertical channel. This is the simplest configuration to allow the key phenomena of a static residual wall layer to occur and to study the competing effects of yield stress, buoyancy stress, viscous stress and viscosity ratio.

More rheological complexity can be introduced through consideration of two Herschel-Bulkley fluids, and this should be done, to represent cementing fluids more completely, although we do not anticipate significant qualitative changes in the results. On the other hand, in the annulus context well inclination is expected to have a significant effect on displacement efficiency. Recent progress has been made on horizontal channel displacements by Eslami et al (2017). However, we are still far from complete in terms of the parameters to be understood.

Problem 2: Fluids invasion

In this second problem we have studied the mechanism by which a fluid invades a column of gelled fluid under pressure, through a single isolated pore (hole). This is an archetypical setup for gas invasion. Here our focus is on the effects of fluid type, yield stress of the invaded fluid and column height on the invasion process. We have studied both miscible liquid-liquid invasions (Zare et al, 2016) and immiscible liquid-liquid and gas-liquid invasion (Zare & Frigaard, 2018a).

To motivate the direction of our study, note that cement slurries are considered to be yield stress fluids within the oil & gas industry, typically with a yield stress of 5-15Pa, and are placed in long annuli. One theory advanced for how the yield stress may aid fluids invasion is that following the volume loss during hydration, the annular cement is pushing downwards. This downwards pressure gradient is resisted by the yield stress, at the walls of the annulus, and this in turn reduces the hydrostatic pressures in the annulus. Thus, the yield stress and length of annulus are important in assessing the pressure reduction. By the same reasoning, if fluids invade this means that a volume of fluid is added to the annulus and the in situ fluids are displaced upwards. This upwards displacement can only happen if the yield stress is exceeded. Indeed, any displacement of a fluid volume all the way to surface should require a force that scales with the yields stress, height of column and a lateral length-scale. If we can establish that the yield stress affects the invasion process in this way, then this leads to ways in which to affect fluid invasion.

Methodology

Our main methodology is experimental. From the field perspective, a number of pressures should be considered as active in a fluid invasion scenario: hydrostatic pressure, formation pressure, capillary pressure, buoyancy stress, yield stress, etc… On reproducing this on the lab scale, atmospheric pressure dominates. We remove this effect by using a manometer arrangement, control the pressure differential by varying the height of the invading fluid column and then are left just with buoyancy, capillary and yield effects. By studying an initial configuration with horizontal interface, buoyancy does not create shear, and can also be eliminated by density control. We can then eliminate capillary effects by initially studying a miscible fluid pair, which allows us to focus on the yield stress effect of the invaded fluid.

Figure 20 shows a schematic of the experimental setup. The invaded fluid was placed in a cylindrical column (1.25” radius R x 25” length L), and invasion occurred through a hole of 1/100th the column radius. The invaded fluid was a solution of Carbopol (a common water-based yield stress fluid), mixed in 3 different concentrations (which controls the yield stress). The height H of Carbopol was adjusted between experiments, but in each case the space above the Carbopol was topped up with water, to give the same static pressure on the invaded fluid side. The invading fluid fills a tube attached to the invasion hole at the bottom of the column, and is connected to a reservoir of invading fluid which is mounted on a scissor jack. Varying the height of the scissor jack allows pressure variation to a precision of 0.001 Pa, although the actual measurement of pressure is visual – from the height of the reservoir surface.

The fluids are characterized via their density and rheology, but the main measurements of the experiment are visual. Carbopol is transparent and we can colour the invading fluids with dye in order to observe the behavior of the front as the fluid penetrates, We also use fluorescent dye and a laser sheet in order to visualize invasion along a central plane of the apparatus. A full description of the setup and method can be found in Zare et al (2016) and Zare & Frigaard (2018a).

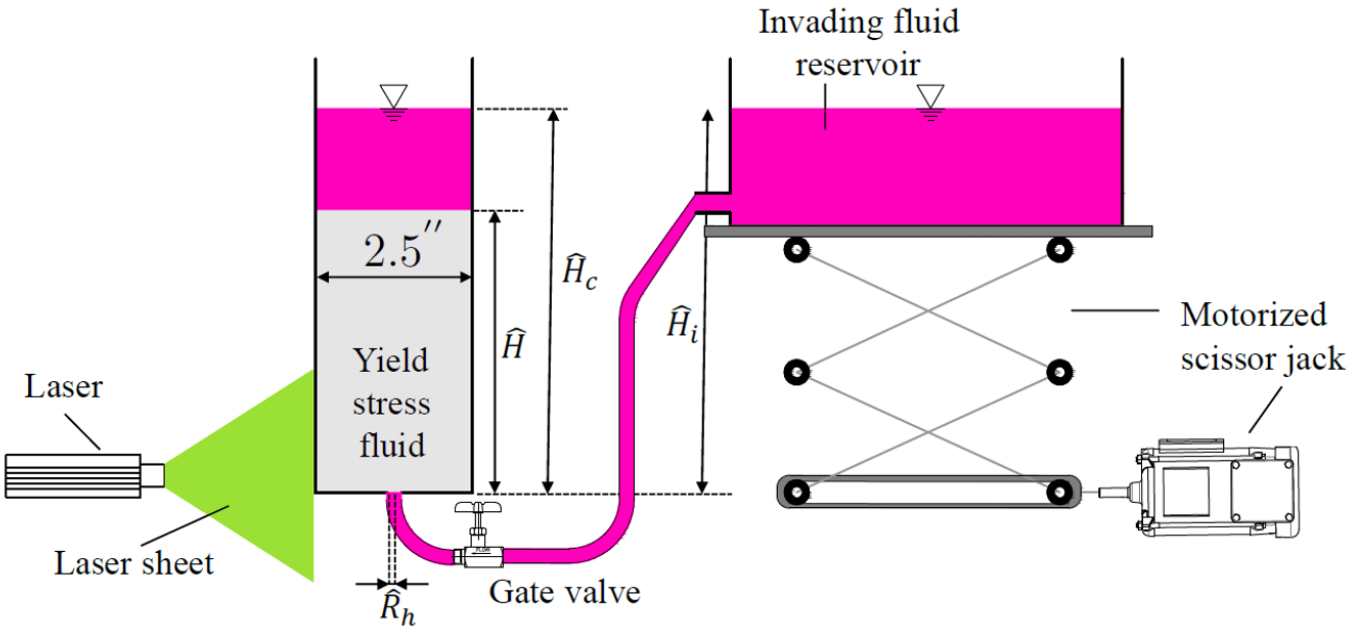

Figure 20: Schematic of the experimental setup used

It is worth commenting that the apparatus used and described in Zare et al (2016) and Zare & Frigaard (2018a), was only arrived at by a process of continual improvement/refinement to ensure repeatability. It is helpful to understand some of the choices and false direction taken, i.e. to avoid the same mistakes for other researchers.

- Our initial thought was to simply use an air line with pressure regulator. Fine control of air pressure requires expensive medical-quality regulators to attain 1 Pa – scale precision, and most of the control is wasted on balancing atmospheric pressure. The manometer design is easier.
- We also started with air injected via a needle inserted in the middle of the column. The flow was dominated by bubble growth and detachment – both governed by high (capillary) pressure scales and buoyancy was quickly evident in the bubble formation.
- There are often debates about measurement of yield stress, i.e. how and to what precision? To minimize variations we kept to the same consistent preparation of fluids throughout and fixed at just 3 concentrations (yield stress values). Variability of the experiment is better controlled by changing the height H of yield stress fluid and by varying the pressure imbalance through the reservoir height.
- Although hole size is an interesting variable, we kept this constant for all experiments. For immiscible fluids, with a small hole capillary effects quickly become dominant. Also there were effects to avoid in the experiment, such as blocking the hole with yield stress fluid.
- Due to questions about potential slip at the walls, we applied a special coating to the plexiglass container to avoid this. It was probably unecessary, as we never saw any tendency for the invading fluids to migrate along the wall.
- Initial experiments used ink instead of flourescent dye. The latter exposed more features of the flow close to the invasion hole, but the ink was nice for visualizing the post-invasion propagation
- We experimented initially with rectangular columns for the yield stress fluid column, then when we found that the post-invasion proagation of the invading liquid was quite asymmetric, we decided to use a symmetric circular cylinder

A photo of the apparatus in some of its earlier iterations is given below in Figure 21.

i. Air is injected into carbopol. Injection pressure is controlled with pressure regulator.

ii. Controlling injection pressure with manometer.

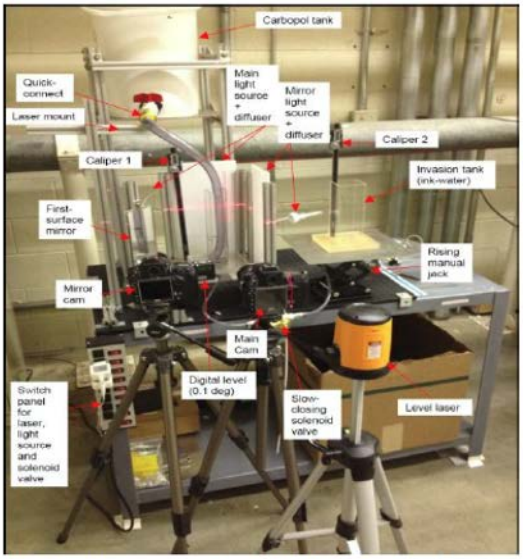

iii. Invasion pressure is controlled by making difference in fluids level. The height difference is applied with lifting up the column of water by a scissor jack under the water tank.

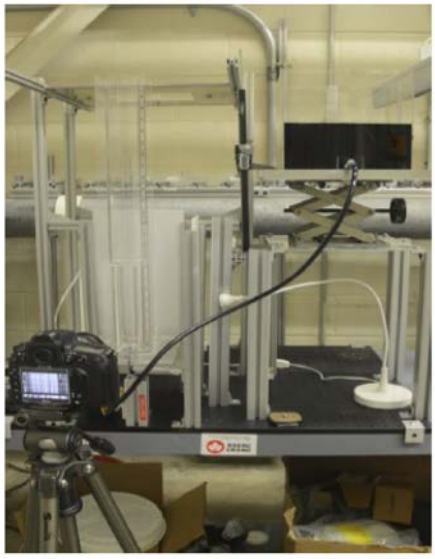

iv. Change the size of water tank and increasing the length ratio of the tank to 10.

Figure 21: Photos of the experimental apparatus during its development (i) – (iv)

Results and Data

The first analysis that we have performed for the experimental setup is a dimensional analysis. In this we subtract off the static pressure and scale the remainder through with the yield stress. This leads to the statement that invasion will occur when the dimensionless hole pressure P_h exceeds an invasion pressure limit P_i which can be decomposed into two components: a yield stress component and a capillary component, i.e. invasion occurs when:

$$P_h > P_i = P_Y + P_{it}/Ca_Y, \qquad (1)$$

where $P_Y = P_Y(H, r_h, Ca_Y)$ is the yield component and $P_{it} = P_{it}(H, r_h, Ca_Y)$ is the interfacial tension component. The dimensional hole pressure is $\hat{P}_h = \hat{\rho}\hat{g}\hat{H}_C + \hat{\tau}_Y P_h$, where the hat accent denotes a dimensional quantity:$\hat{\rho}$ is the density, $\hat{g}$ the gravitational acceleration $\hat{H}_C$ the total height of liquid in the column and $\hat{\tau}_Y$ is the yield stress. The parameters H and r_h are the height of yield stress fluid and the hole radius, both scaled through with the column radius $\hat{R}$. Finally, Ca_Y is the capillary yield number: Ca_Y=$\hat{R}r_h\hat{\tau}_Y/\hat{\sigma}$, where $\hat{\sigma}$ is the coefficient of interfacial tension. The above expression (1) is deduced from a continuum mechanics description of the invasion process, considered as a static problem, e.g. viscosity is not important until invasion (motion) occurs.

This description was useful in breaking the problem into small pieces. In the first place, if we take miscible fluids e.g. water invading Carbopol, then we have $Ca_Y = \infty$, and we can focus only on the yield component P_Y, determining $P_Y(H, r_h, \infty)$, and we might hope that the interfacial tension does not affect the yield component. This was our first set of experiments, in Zare et al (2016). We then considered other miscible and immiscible fluids in Zare & Frigaard (2018a).

Miscible invasion

In our experiments we initially balance the heights of the fluids using a laser level, and then we slowly increased the height of the reservoir of invading fluid, so as to increase $\hat{P}_h$ until the point of invasion. Instead of seeing a clear invasion instant, we discovered that invasion seemed to have a number of complex stages, which are illustrated in Figure 22.

- ***Mixing stage***: A very small mixed region of water-carbopol develops directly above the hole. The water is observed to mix into the carbopol, but there is no observable motion of the fluids i.e. no displacement. This stage is probably driven by either molecular diffusion or osmotic pressure. The precise extent of the region is hard to specify as it is diffuse, but a typical thickness is ~0.1mm.
- ***Invasion stage***: At the center of the mixed region, when the pressure is high enough, the water advances into the mixed region of the carbopol column (*invasion*). Typically the invasion takes the form of a minuscule dome appearing directly above the hole, (≈0.5mm radius for water). Within the dome the intensity of the LIF image is significantly brighter than in the diffuse mixing stage. If the pressure is not increased further, the mini invasion dome becomes progressively diffuse but does not grow. Therefore, the applied pressure is increased beyond the invasion point at the same ramp rate. The dome increases with pressure, but also up until this point invasion and deformation of the Carbopol is regarded as elastic, i.e. if the pressure was reduced the mini dome would shrink back and apart from diffusive effects this invasion is reversible.
- ***Transition stage***: The invasion stage continues until the small invasion dome is observed to oscillate and becomes significantly brighter. At this point the reservoir height is held constant: the pressure is not increased further. The invasion pressure $\hat{P}_i$=$\hat{P}_h$ is then recorded. These phenomena signify the onset of a second stage of

the invasion, that we have called the *transition* stage. During transition, the small invasion dome expands and it seems that the surrounding fluid has plastically yielded. Although there is a flow into the dome from the reservoir, the change in static pressure balance is negligible and the applied pressure at the hole can be regarded as constant. The dome expansion eventually slows as the dome expands, signalling the end of the transition stage. The interface of the dome ranges from being visibly *smooth* (if the applied stress is relatively large), to *granular* if the applied stress is small. This surface variation is illustrated in Figure 23.

- ***Fracture stage***: At the end of the transition stage, a small finger or non-uniformity is observed to initiate a *fracture* of the dome surface. This either happens at the transition pressure, or after a slight further increase in applied pressure (needed only if the dome remains stable at the end of transition). During the fracture stage the water advances away from the dome in a dyke-like sheet, the edge of which can both finger and branch as it advances, see Figure xx.
- ***Arrest stage***: With no further increase in static pressure to drive the flow, eventually the invasion flow stops. Stopping is dependent on the carbopol height. Either the invading water penetrates fully to the surface of the carbopol or it may stop before reaching the surface.

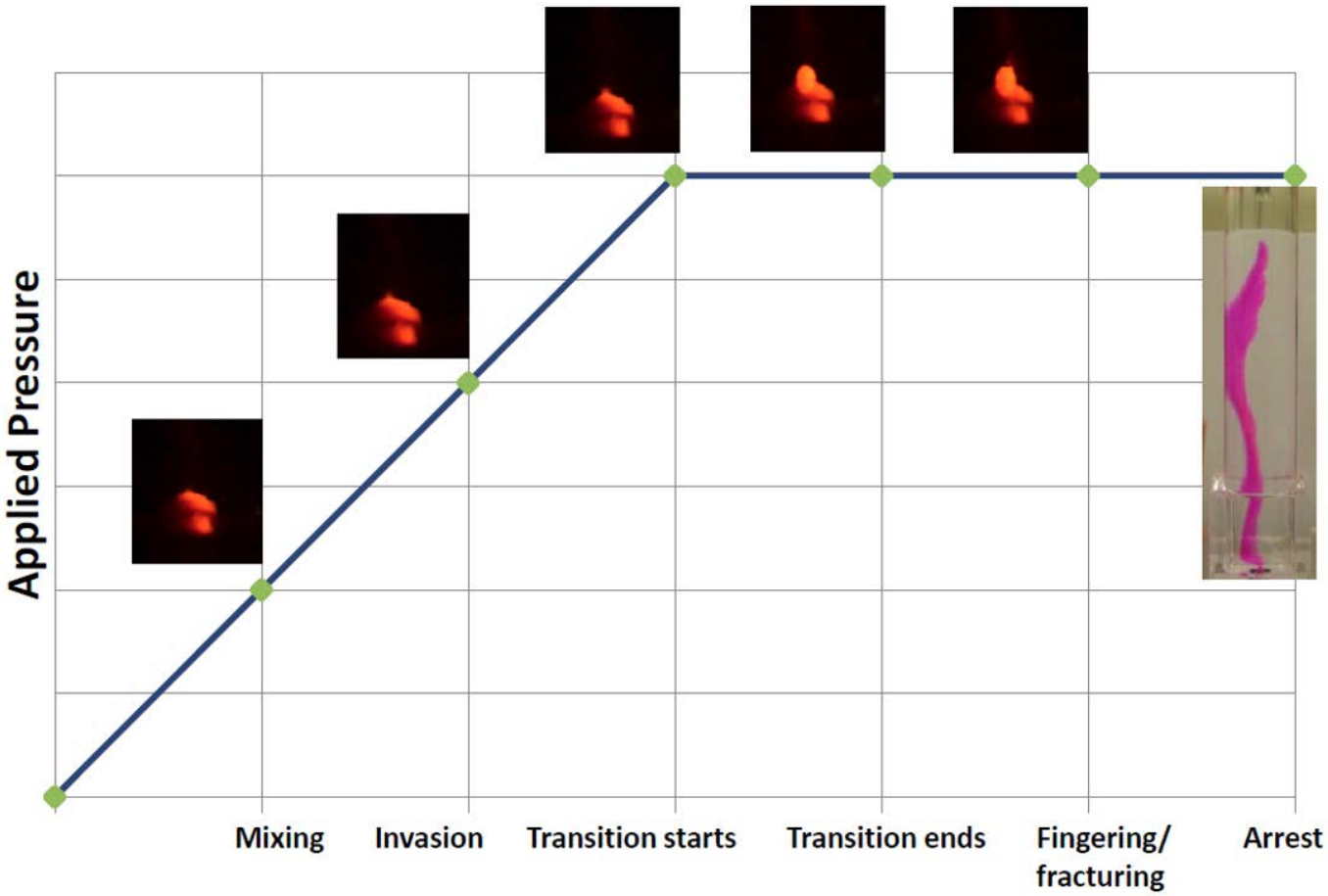

Figure 22: Different stages occurring in a typical miscible invasion

Broadly similar stages were followed in our later experiments using glycerol solutions. Here we used 2 different concentrations (G45 = 45% and G58 = 58%), which resulted in both density and viscosity changes. The increased density meant that the final fracture/arrest stages proceeded with the fracture/dyke remaining in the bottom of the column, i.e. due to density; see Figure 25.

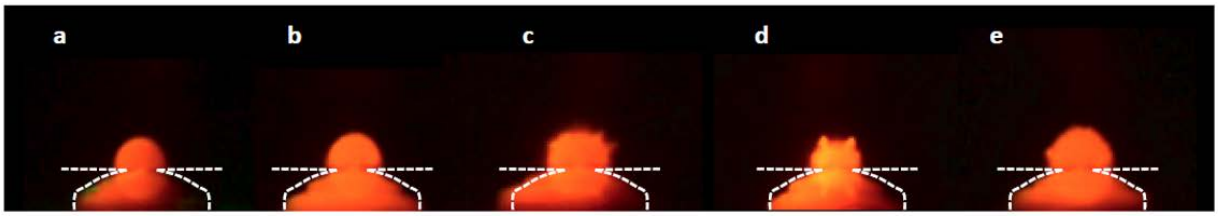

Figure 23: Examples of different invasion domes after transition, ranging from smooth (a & b) to granular (c-e). The white broken lines are a guide to the eye for the bottom surface of the tank and the machined hole.

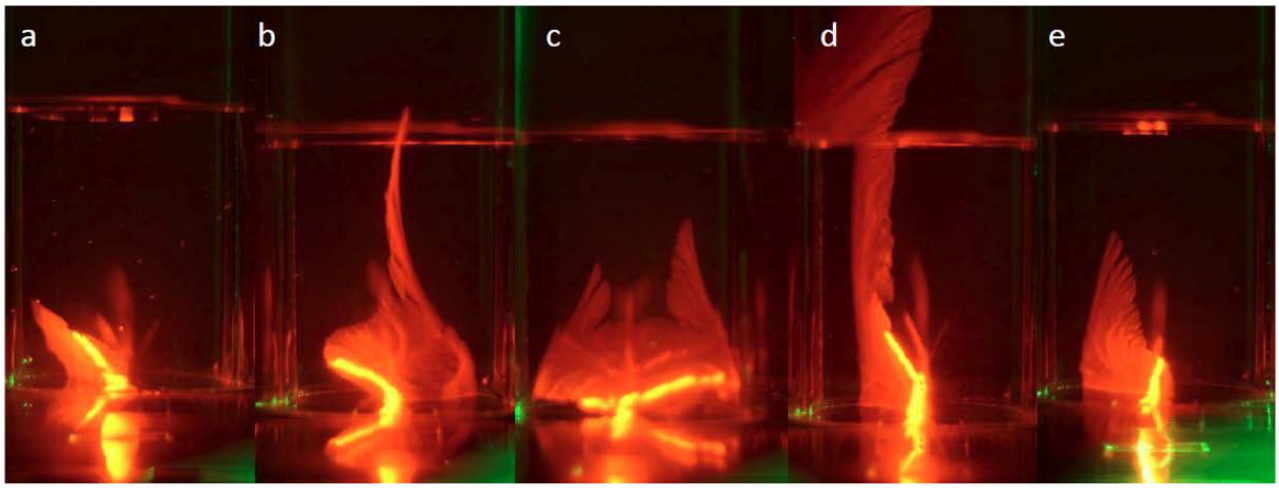

Figure 24: Examples of post invasion propagation in the fracture stage (from Zare et al 2016)

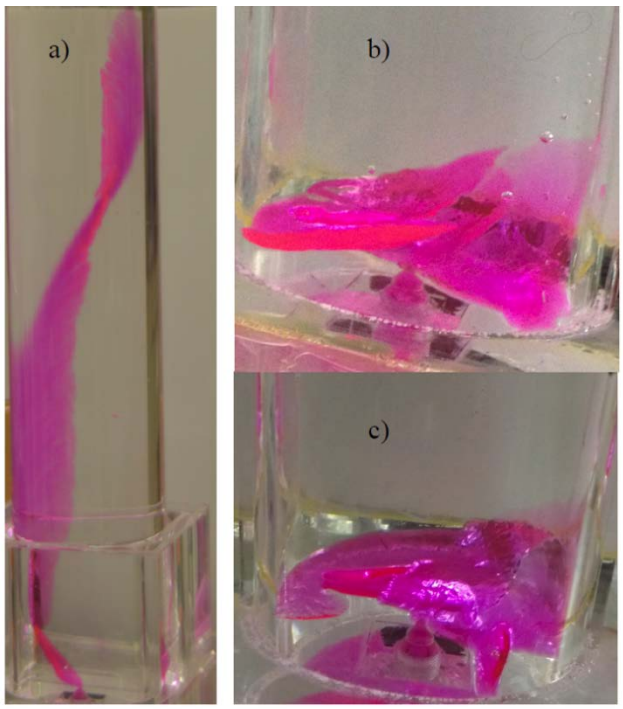

Figure 25: Post invasion propagation in the fracture stage, with a) H2O, b) G45, c) G58; (from Zare & Frigaard 2018a)

The miscible invasion experiments revealed some differences between H_2O (water) and G45 & G58 (glycerol) invasions. The main observable one was that the transition domes were significantly larger for G45 & G58 than H_2O. In both cases, the domes were approximately axisymmetric and in the case of G45 & G58 showed no observable slumping/spreading, indicating that density differences were not a factor in the invasion.

After some investigation, it was found that the G45 & G58 also took significantly longer to get to the invasion stage. As the starting point for the experiments was a similar hydrostatic balance and the ramp rate of the scissor jack was the same, this longer time before invasion just meant that the hole pressure had built up further. As the transition seemed to involve a form of relaxation and local yielding of the Carbopol, the larger domes are perhaps just related to the larger pressures. The reason for the longer time spent in the mixing stage is unclear. The mixing stage seems to be related to weakening of the gel at the scale of the gel particles/grains, and by a diffusive or osmotic process. The G45 & G58 will have higher viscosity and hence smaller diffusivity, which may slow these processes. Further investigation would be needed to determine this, and perhaps a more targetted experiment.

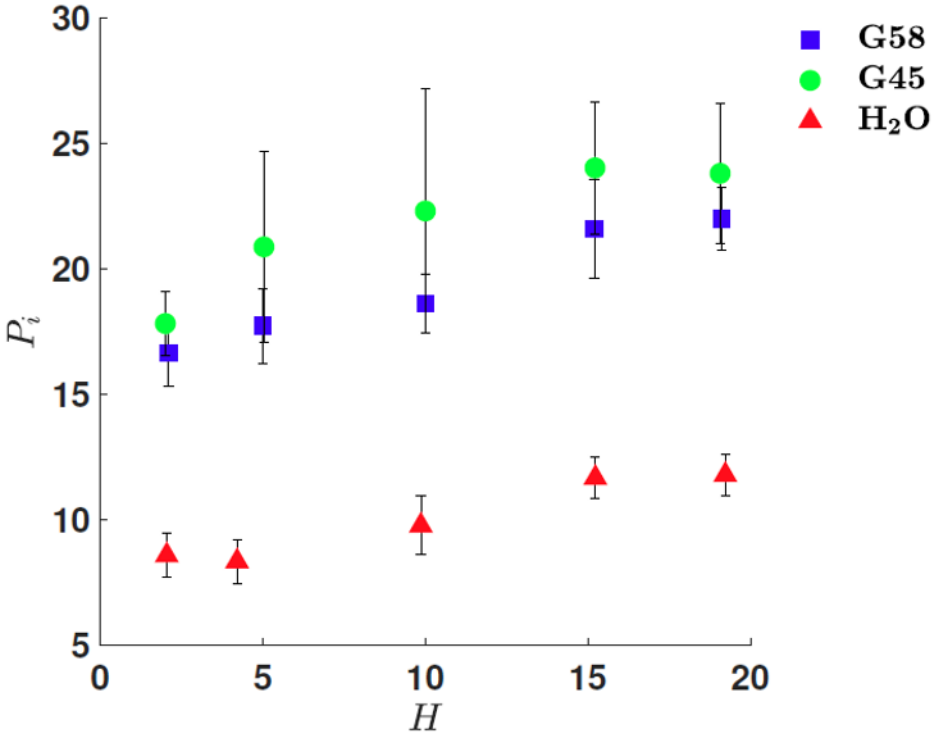

Figure 26: Dimensionless invasion pressures for H2O, G45 & G58; (from Zare & Frigaard 2018a)

Directly related to the above discussion, the dimensionless invasion pressure for G45 & G58 was significantly higher than for H_2O. For all of these fluids we observed a mild linear increase in P_i with H. This confirms the fact that (in dimensional terms) both the height and the yield stress contribute to the increase in invasion pressure.

However, the increase in P_i with H was significantly less than $P_i = 2H$, which is the limit one would expect in displacing a pipe full of yield stress fluid. This is because the invasion process appears to happen in a very local way, from the initial mixing and invasion stage right through to the fracturing/fingering. We also carried out a range of computations (see in Zare et al, 2016), which confirmed that for small holes the first yielding would be local, and only for larger holes do the invasion pressures follow, $P_i = 2H$.

It is perhaps surprising to see the large error bars in Figure 26, in what may initially appear a simple experiment. Part of that variability comes from repeated experiments. Each height was repeated with the different Carbopol solutoions and each experiment repeated typically 3 times. Repeatability of the rheometry was good, i.e. very similar flow curves were obtained. However, the flow curves are then analysed to produce the yield stress value used for scaling pressures. This gives some additional variability in the data. The other part of the variability comes from the measurement and interpretation of invasion, which we have defined as the end of the invasion stage/beginning of transition stage. As discussed, this is a form of elastic-plastic yielding that we are trying to capture by inferring from visual measurements of the dome as it is *about to change*. This is not a *strain gauge,* with experimental geometry designed to capture a single component of stress or strain and the inherent nature of yielding is sensitive to material and geometry. The variability is mimicked in the range of dome sizes found for each fluid – see the panoramas of transition domes illustrating this in Zare et al (2016) and Zare & Frigaard (2018a).

Immiscible invasion

Immiscible invasion experiments were conducted with 2 fluids. Rhodorsil oil (BLUESIL FLD 550 from Bluestar Silicones; R550) and air. The R550 is a silicon based oil with density slightly more than water and viscosity about 125 times larger. To eliminate any density effect, we weighted the Carbopol solutions with a small amount of glycerin, i.e. so were exploring interfacial tension and viscosity effects. In considering air, we of course have a density difference, smaller viscosity and a more significant interfacial tension.

For R550 the main effect of viscosity appeared to be that the experimental fluid motions were significantly slowed. Thus, the constant pressure ramp was replaced by a stepped ramp in which we waited periodically at different pressure levels to see if the fluids were moving before increasing reservoir height again. The main difference in the R550 invasion was that the invasion fluids had no mixing stage and no mini-invasion dome. Once invasion started the dome grew continuously. Figure 27 shows one such invasion sequence.

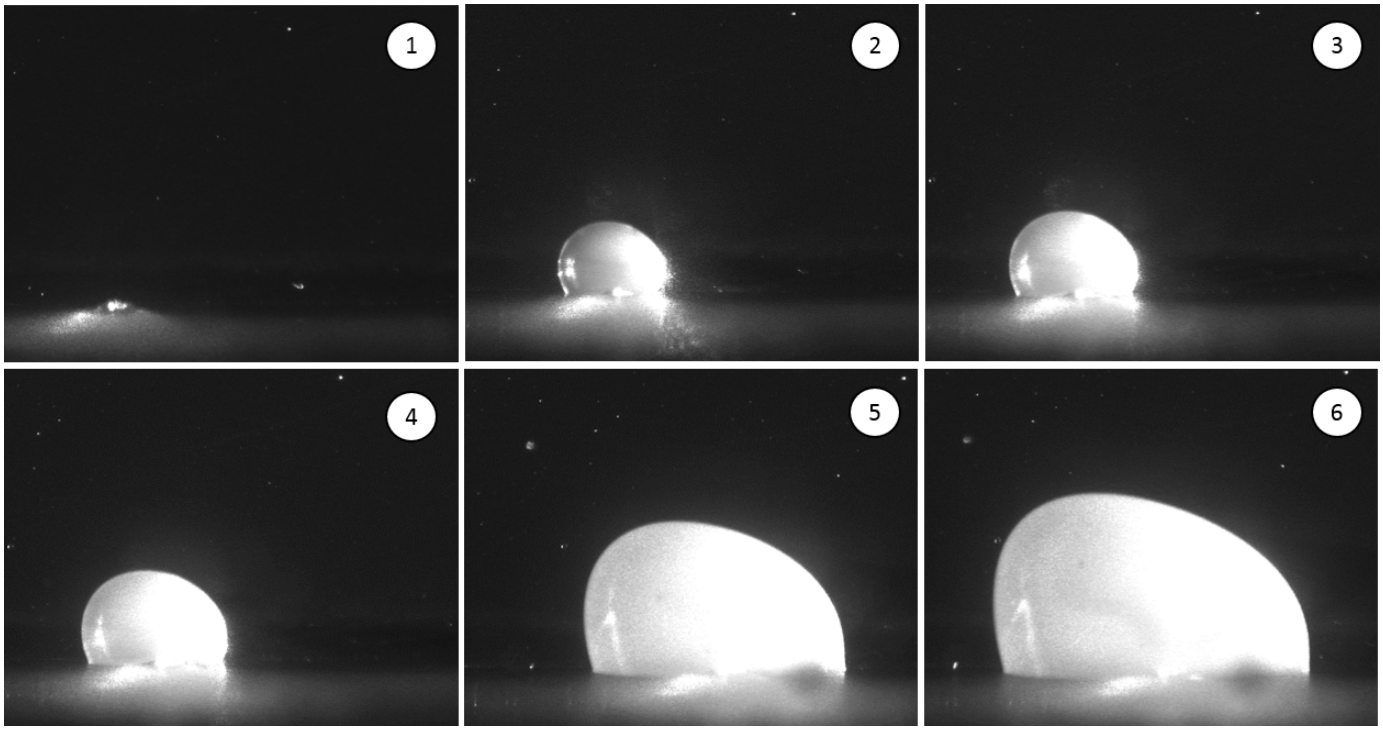

Figure 27: Example invasion of R550 into a density matched Carbopol solution

Also notable is that there was no rupture/fracture stage in these invasion experiments. Indeed, when left for sufficient time the dome simply expanded to fill the entire cross-section of the column. In our experiments this could be very slow (i.e. even being left overnight at the transition pressure), and probably this is due partly to the small diameter tube used to connect the reservoir to the invasion hole. An example of a later stage in an R550 experiment is shown in Figure 28. The morphology of the domes is different to the miscible fluids, but they are not entirely hemispherical (see Figure 27). Probably the high viscosity dominates the flow and this means that the shape evolves away from axisymmetric as it grows.

Figure 28: Invasion of R550 into a density matched (0.15% wt) Carbopol solution of height H=10 radii

The exciting aspect of this flow is that the invasion was non-local. There was no weakening of the gel structure via mixing/diffusion and invasion essentially displaced the entire column upwards. Figure 29 shows the invasion pressures for R550. The black broken line has slope 2, i.e. is equivalent to the Poiseuille flow curve where the Carbopol column yields at the wall. This fits much better with our dimensional analysis and suggests that at least for some fluids we are able to separate yield and interfacial contributions.

The air invasion experiments were different again. For these there was again no mixing stage in the invasion. Once the invasion started, it proceeded continually. However, here the effects of buoyancy were evident. Although the initial invading dome was hemispherical (capillary controlled), as this grew buoyancy quickly elongated the shape into a long bubble. The scale of the bubble was always larger than the granular scale of the gel and at no point did the interface lose its smooth and crisp appearance, i.e. throughout the invasion interfacial tension, seemed to suppress any local effects on the granular scale. The strong buoyancy (and possibly the viscosity ratio) meant however that the bubbles formed advanced up through the centre of the column in all cases, i.e. they did not

displace the entire cross-section of the Carbopol column. We see in Figure 29 that the invasion pressures did not vary significantly with H. Also however, we note that the increase in P_i is significant. This increase cannot be accounted for purely by the increase in interfacial tension $\hat{\sigma}$ (approximately double). By a series of additional experiments (detailed in Zare & Frigaard 2018a) we were able to determine that approximately half of the increase is directly due to interfacial tension. The remaining half comes about via a combination of interfacial tension and yield stress, i.e. the local yielding of the Carbopol is made harder by the interfacial tension, which prevents the air from diffusing/mixing at a granular scale.

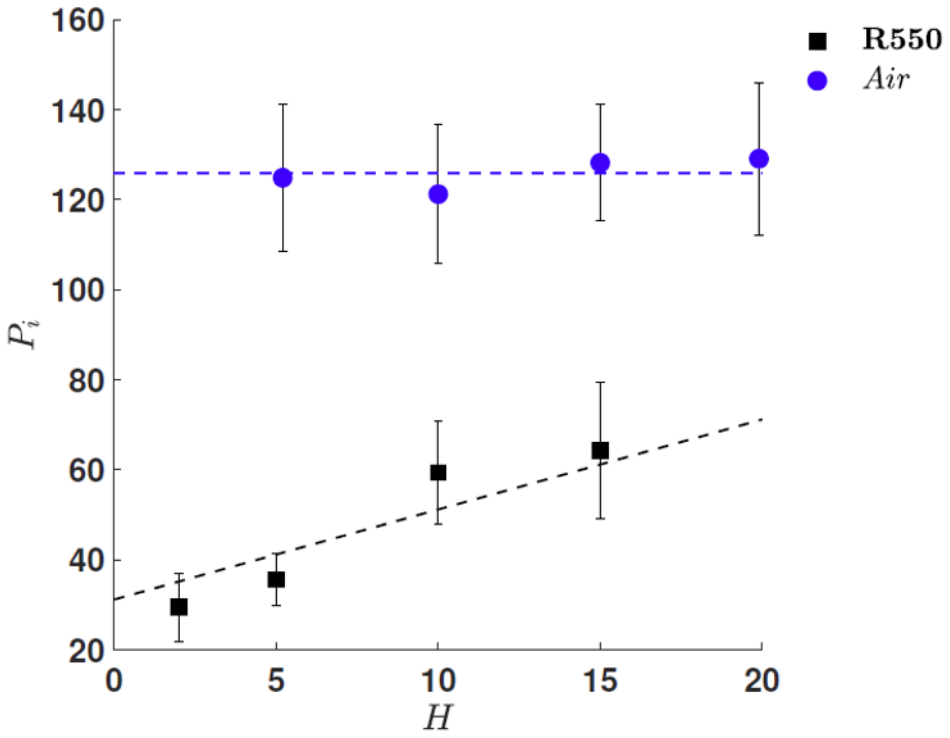

Figure 28: Dimensionless invasion pressures of R550 and air

Further experiments are detailed in Zare et al (2016) & Zare & Frigaard (2018a), e.g. propagation of the bubbles, weakening of the gel by repeated invasion.

Discussion and Conclusions

We have presented new results targeted at exposing the effects of the yield stress on the pressure P_i required for one fluid to invade a column of another fluid, through a small hole. This setup was designed to simulate invasion into a well during primary cementing (or even other operations when the wellbore fluid is stationary), for relatively low porosity reservoirs where pores may be considered isolated, e.g. in our experiment the hole radius was ~1% of the column radius.

The invaded fluid was a Carbopol gel, mixed in 3 concentrations. Approximately 400 experiments were performed, repeatedly covering 3 different carbopol concentrations and various heights of column for 3 miscible invading liquids, 1 immiscible liquid and air. The study was constructed so as to isolate effects of the different potential stress contributions to the force balance determining invasion. This was supplemented by a computational study.

For low column heights $H \sim 1$ (i.e. height similar to column radius) there is little effect of H but as H increases we observe a steady approximately linear increase in P_i over the experimental range. Dimensionally, P_i measures the invasion over-pressure (i.e. pressure above the hydrostatic pressure in the fluid column), scaled with the yield stress. Thus, our results show approximately linear increase with H in required over-pressure for invasion. Also the invasion over-pressure increases linearly with the yield stress, as follows simply from the scaling adopted.

The experiments show significant variability, hence the repetition at each height and carbopol concentration, despite considerable evolution in the experimental procedure to reduce this. For example, we have carefully implemented protocols for fluid preparation, tank filling, eliminating invasion hole plugging, etc..., and have eliminated buoyancy, capillary, static and atmospheric pressures via our experimental design. The remaining variability stems from the fact that we are measuring an isolated onset event in a dynamically evolving process, and that this event is identified phenomenologically by the appearance of a minuscule invasion dome and then by the growth of that dome to a transition point that we believe to represent elastic-plastic yielding.

A number of interesting stages have been observed during the experiments: *mixing*, *invasion*, *transition*, *fracture* and *arrest*. The passage from invasion to transition pressure seems to represent elastic-plastic yielding close to the invasion hole. The initial growth of the transition dome and then slowing of growth (in cases where the fracture does not start immediately) suggests a relaxation of the stress field, due to the overpressure now being applied over a larger area. We have seen that the expanding dome interface can be either relatively smooth or granular. This does not appear to have any bearing on the stability of the transition dome: either may be stable or unstable. Invasion and transition domes are approximately axisymmetric. Fracture initiation and propagation represent a departure from symmetry, probably due to either a local defect or a non-uniformity of the stress-field.

Our tests with glycerin solutions, comparing against the water invasion studies revealed the following: (i) the glycerin solutions have a slower mixing/invasion stage (longer times before transition); (ii) invasion pressures are consequently higher; (iii) after transition the invading domes grow more rapidly and are significantly larger than those for water at the point when fracturing initiates. These differences are partly attributed to the larger viscosities of the glycerin, which we believe slows diffusive/mixing processes. On the other hand, there are many similarities to the water invasion studies. The invasion stages are similar and invasion is a strongly localised process. The increase in P_i with H is also far slower than the Poiseuille flow limit ($= 2H$). The transition point also appears to be associated with elastic-plastic yielding of the Carbopol.

We found no significant effect of the density difference on the invasion pressure, which is consistent with our dimensional analysis. Two glycerin concentrations were used (G45 and G58). It was noted that the invasion pressures and dome sizes were larger with G45 than G58, whereas the larger concentration would be expected to have the lower diffusivity as it has higher viscosity. This was therefore unexpected, although these differences lie within the error bars of the data, and we have no obvious explanation. Another phenomenon noted in the larger glycerin domes was a recirculating secondary flows, which appears to entrain Carbopol into the invading fluid. These flows were not observed in the smaller domes. Following invasion and rupturing of the dome, the glycerin solutions propagate in dyke like fractures that are thicker than those for the less viscous water and which slump towards the bottom of the invasion column (presumably under gravity).

Our computational study has covered a range of invasion hole sizes and dimensionless heights H. Results are not presented in this report, but can be found described fully in Zare et al (2016). The computed invasion pressures follow similar qualitative trends to the experiments but are themselves over-predicted. This is probably due to the ideal visco-plastic (Bingham) law that we have implemented. The computations also reveal that the invasion pressures for small hole radius increase relatively slowly with $H > 1$. This is tied into the occurrence of a local dome-like region of yielding close to the hole, i.e. the invasion overpressure first causes fluid to yield and recirculate locally within a dome shape, that appears analogous to those observed during the transition stage.

As H is significantly increased, for small hole radii, the increase in P_i eventually generates sufficient stress to reach the walls of the cylinder. After this, the invasion process changes from a local phenomenon to a global one, in which resistance of the fluid occurs on the scale of the cylinder. More specifically, there remains an $O(1)$ region close to the hole within which the magnitude of the deviatoric stresses components are all significant. The stresses generally decrease away from the hole, but at sufficiently large H yielded fluid does extend to the wall. Above this local near-hole region, the fluid adopts essentially a Poiseuille profile, with linearly decreasing shear stress from centre to wall. Hoop and extensional stresses, which are important in the near-hole region, decay in the Poiseuille region as H is increased.

We further observe that the invasion pressure increase proceeds in parallel to the Poiseuille prediction ($P_i = 2H$) both for small holes at sufficiently large H and for larger hole radii. For the larger hole radii there is no range of H for which yielding is local and isolated, instead the Poiseuille regime is entered immediately. Returning to the experimental results, the invasion pressures increases at a rate that is significantly below $P_i = 2H$. This, the hole size and the phenomena observed, all suggest that our experiments are fully in the local regime of invasions. The initial domes are approximately axisymmetric and apart from exhibiting elasticity and a more complex constitutive behaviour the computational and experimental results present a coherent picture.

We have presented new results governing the invasion of fluids into a gelled static column of yield stress fluid. Our initial dimensional analysis ignores miscibility effects and suggests that the invasion pressure P_i should depend on H, dimensionless hole radius and the yield capillary number Ca_Y. The hole and column radii do not vary within our experiments and we have split P_i into a yield pressure part and an interfacial tension term (scaled with $1/Ca_Y$). Our results show that this splitting is problematic unless miscibility effects are better understood, but otherwise serves as a useful conceptual framework.

Our experiments with immiscible fluids involved a density matched silicon oil (R550) and air. It was immediately apparent that interfacial tension had a large effect on invasion. Our experimental protocol was changed to increase the invasion pressure in larger steps than for the miscible fluids. Mixing was eliminated as was the occurrence of an initial micro-invasion dome. Instead, once invasion started we observe a clear interface expanding into the Carbopol

column. In the case of the R550 the interface evolved as an approximately hemispherical dome, slowly filling the bottom of the column. The invasion pressure was significantly larger than for the glycerin solutions and was non-local in that it was resisted by yielding at the walls of the column, with P_i increasing as the Poiseuille flow $2H$.

The air also did not mix and had no micro-invasion dome. However, the invasion was localised in the sense that buoyancy dominated after any significant influx, leading to the invading fluid stretching upwards into a long bubble, which eventually detached and propagated to the surface. Thus, resistance of invasion at the walls did not occur and P_i was approximately constant with H. Also the measured P_i was much larger for air than for R550. Further analysis of this increased P_i suggested that about 50\% of P_i is directly attributable to interfacial tension and the remainder to yield stress. However, the yield stress is only able to resist effectively when there is no mixing/diffusion.

Regarding the cementing process, quite a few aspects of our study appear relevant. Firstly, the complex behaviour of P_i with H and secondly the change from local to non-local invasion. Here we neglect effects of any filtercake that may have formed during drilling. Although H is very large in the wellbore setting, pore size is also very small. Taking a typical annular gap as the global scale, pore sizes in the sub-micron range are very likely to invade locally. This will also depend in a significant way on the porosity, which can also be interpreted in terms of the hole/container radius ratio, i.e. at larger porosity values the pores can no-longer be considered as isolated: local invasion domes influence adjacent pores. Our computed results suggest that in the cylindrical geometry this happens for a radius ratio > 0.1.

Secondly, a different perspective on local/non-local yielding comes from the observations of smooth and granular surfaces in our transition domes. Here the scale of the granularity appears to be in the range of 1-100μm, which may be related to the carbopol gel microstructure and its stress response on this scale. In the well, cement slurries are in reality fine colloidal suspensions and pore sizes in tight rocks extend down to the scale of the suspension microstructure, (indeed in such rocks it is not uncommon to consider Knudsen effects on porous media flows). Thus, local invasion on the scale of the slurry microstructure is likely to be the norm in cementing and this requires separate study using real cements.

Thirdly, the influence of the yield stress in linearly increasing invasion over-pressure is useful, if also anticipated. If the invasion is local then the critical point is that it may occur at significantly lower pressures than those predicted from non-local analyses, e.g. predicting flow in the annular gap. If however yielding is local, with recirculation of fluids close to the pore opening, many other effects may influence the potential and mechanism for annular fluid to exchange with the pore fluid, and the timescale for that exchange, e.g. buoyancy, capillarity, diffusion, osmotic pressure... These effects have not been studied here. In the same context, note that here we have tried to eliminate local variability in our experiments, but in any cement placement process (and in the drilling process) the wellbore is over-pressured. Thus, yield stress fluid is forced into the pores, filtercake/skin typically forms close to the borehole, and these effects may in practical situations be the main influence of the yield stress on the actual invasion stage.

Next, in the above context - if we are to assume that local invasion occurs and that local gas streams coalesce, an interesting fluid mechanics problem to consider would be the propagation of a large gas stream upwards through an inclined annulus of stationary yield stress fluid. Although in our simple setup we have shown the relevance of Poiseuille flow-like bounds, in inclined eccentric annuli the gas path is less predictable and may exchange/by-pass in situ fluids as it rises up the annulus.

Comparatively, we see that invasion of miscible fluids is the least affected by either the yield stress or the height of the column. The invasion process is strongly localised and retarded by an increased viscosity. In the well context,

this suggests the largest vulnerability to formation brines, rather than hydrocarbons. Brines may affect the cement hydration locally, but probably do not represent any migration risk.

Interfacial tension has a significant role to play in conjunction with the yield stress. The interfacial tension prevents local diffusion and weakening of the gel structure with subsequent invasion on this scale. This allows the yield stress to resist on macroscopic scale. Thus, for example we might expect additives that increase the yield stress of the slurry to be effective in preventing oil invasion. The principal difference between air and R550 in our experiments was the domination of the air invasion by buoyancy. The initial invasion was similar and dome like, but air invasion migrated upwards which prevented the dome from growing outwards to the wall. We might expect a similar effect in a well. Thus, although the gas invasion pressure may be significantly higher than that for water or oil, it seems to be largely independent of H: once entered into the annulus reservoir gas will channel upwards through the cement slurry, rather than displace it. We suggest that effective cement additives for gas invasion would need to force the invading gas pockets to expand locally and displace the entire annular cross-section. In this way rheological contributions to P_i that scale with H can be realised. For example an additive that quickly develops viscoelastic properties in the liquid phase of the cement (i.e. downhole bubblegum), is likely to be more effective at preventing invasion than a pure yield stress effect alone.

Recommendations

The two projects have been quite different in scope, but both are research projects targeted at development of fundamental physical understanding of underlying gas migration processes. This is pre-commercial research and not necessarily directed at any product. The nature of the research results are such that they should be incorporated as part of an overall improvement in process design. It is for the different respective stakeholders to integrate this knowledge into design or execution procedures in the way most appropriate, e.g. potentially as part of a physical software model or perhaps to give ideas for a product. Here we focus primarily on research recommendations for continuation.

In terms of priority areas for continuation of project 1:

1) Additional research to understand the temporal aspect of wall layer drainage, i.e. moving layers, and how this impacts displacement at different depths in the cemented interval.
2) Consideration of how to integrate the results with existing design tools. In particular, at UBC and in a number of companies, there are annular displacement simulators which model the entire annular displacement. These models calculate wall shear stresses throughout the well, but lose resolution in only dealing with gap-averaged quantities rather than variations across the gap. It would be of value to combine these approaches.
3) In the same direction, some effort needs to be put towards studying annular inclinations other than horizontal and vertical. In particular, we should expect that there will be azimuthal flows close to the interface in any inclined annular displacement, which makes application of our results more complex.
4) Although a large commitment, it would be of interest to run lab-scale experiments directed at the formation of micro-annuli (static wall layers), to see if they are as robust as the models suggest. If successful, the next step would be yard testing with real cements/muds e.g. over the length of a stand of casing positioned eccentrically.

On a longer timescale it would be of value to extend the studies to consideration of two Herschel-Bulkley fluids

In terms of priority areas for continuation of project 2:

1) Having understood the importance of local invasion and miscibility using a polymer hydrogel (Carbopol), we should see how well these conclusions carry over to cement slurry invasion, i.e. a colloidal yield stress suspension. The difficulty here is that we have relied heavily on visualization methods in our experiments, which will be ineffective in a standard cement. This requires some thought and test experiments before moving ahead. A possibility could be to try laponite (transparent, clay-based, thixotropic), then possibly some newer transparent concretes (cement with fine transparent aggregates), and finally cement slurries.
2) It would be of value to experiment with fluid rheologies, to see if we can influence gas invasion to become non-local, i.e. using a visco-elasto-plastic. This type of research could both experimental, testing different materials, but also could be computational, i.e. identifying properties that could then be targeted in materials development.
3) Our experiments to date have firstly, not considered variations in hole size. Secondly, we have operated at a relatively large-scale. It would be of value to develop an apparatus that uses real core samples, or as an intermediate stage uses manufactures arrays of pores, so as to study invasion of different fluid streams.
4) Further up in the annulus, supposing that gas invasion results in a large gas stream, it would be interesting to study propagation along an annulus on the scale of the annular gap, e.g. at different inclinations. Intuitively, one would expect migration along the upper side of the annulus, but this needs to be tested.
5) Lastly, we recommend some study of pore-clogging and how this might be engineered, perhaps in a preflush stage, or with the in situ mud, so as to restrain gas invasion.

Application and Dissemination of Results

As discussed above, direct application of our results requires user-specific development. In terms of the results of project 1, we intend to investigate possibilities for items 1-3 with our own annular displacement models at UBC and will be happy to work collaboratively with other stakeholders to aid their developments. Over the course of the project (and preceding projects), we have disseminated results in the following places, as well as in the PhD thesis of M. Zare (available after examination, end of Summer 2018).

JOURNAL PAPERS:

M. Zare, A. Roustaei, K. Alba and I.A. Frigaard. “Invasion of fluids into a gelled fluid column: yield stress effects,” J. non-Newtonian Fluid Mechanics, 238, 212-223, (2016).

M. Zare, A. Roustaei, I.A. Frigaard. “Buoyancy effects on micro-annulus formation: Newtonian-Bingham fluid displacements in vertical channels.” J. non-Newtonian Fluid Mechanics, 247, 22-40, (2017).

M. Zare, I.A. Frigaard, “Onset of Miscible and Immiscible Fluids invasion into a Viscoplastic Fluid.” Physics of Fluids, accepted for publication and to appear in 2018.

M. Zare, I.A. Frigaard. “Buoyancy effects on micro-annulus formation: density unstable Newtonian-Bingham fluid displacements in vertical channels.” Submitted to J. non-Newtonian Fluid Mechanics, May 2018, under review.

CONFERENCES:

M. Zare, I.A. Frigaard, “Fluid mechanics causes of gas migration during primary cementing,“ Poster presented at BC Unconventional Gas Technical Forum, Victoria, Canada, June 17-18, 2013

M. Zare, I. Frigaard, A. Roustaei, S. Hormozi, Buoyancy effects on micro-annulus formation in primary cementing of oil and gas wells. Presented at AERC 2014, 9th Annual European Rheology Conference, Karlsruhe, Germany, April 8 – 11, 2014

M. Zare, I. Frigaard, A. Roustaei, Formation of static residual layer in miscible density stable displacement. 20th Canadian Symposium of Fluid Dynamics, at the Canadian Applied and Industrial Mathematics Society Annual Meeting, Delta Bessborough Hotel, Saskatoon June 22 to 26, 2014, Saskatoon, Canada;

M. Zare, I. Frigaard, A. Roustaei “Buoyancy effects on forming and removing of residual mud layers during cementing displacements” poster presented at UGTF, Victoria, BC, June 5-6th 2014

M. Zare, M. Ward, Q. Lindfield Roberts, I. Frigaard, “Rheological effects on fluid invasion” poster presented at UGTF, Victoria, BC, June 8-9th 2015

M. Zare, I.A. Frigaard and others “Gel Strength Effects on Fluid Invasion into a Cemented Annuli: Part1” Poster presented at the Unconventional Gas Technical Forum, Victoria April 4-5, 2016

M. Zare, Q. Lindfield-Roberts, M. Ward, K. Alba, I. Frigaard, “Rheological Effects on Fluid Invasion into Cemented Annuli.” Presented at the 9th International Conference on Multiphase Flow May 22nd – 27th 2016, Firenze, Italy (Poster prize winner)

M. Zare and I.A. Frigaard, “Micro-annulus formation in density stable and unstable displacement”. Poster presented at AERC 2017, Copenhagen, Denmark, April 2-6, 2017

M. Zare and I.A. Frigaard, “Capillary effects on fluid invasion process”. Poster presented at AERC 2017, Copenhagen, Denmark, April 2-6, 2017 (Poster prize winner)

M. Zare, “Onset of invasion of miscible and immiscible fluids into a viscoplastic fluid”. Presentation at Viscoplastic Fluids, from Theory to Application 7, Rotorua, New Zealand, Oct 30-Nov 3, 2017

M. Zare, A. Dworschak and I.A. Frigaard “Onset of air invasion into an elastoviscoplastic fluid.” Poster presented at AERC 2018, Sorento, Italy, April 17-20, 2018

M. Zare and I.A. Frigaard “Hydrodynamic instabilities in displacing a viscoplastic fluid with a Newtonian fluid.” Presented at AERC 2018, Sorento, Italy, April 17-20, 2018

M. Zare and I.A. Frigaard, “The onset of fluid invasion and flow development in a viscoplastic fluid” Presented at the Nordic Rheology Conference, June 13-15, 2018, Trondheim, Norway. Included in Transactions of the Nordic Rheology Society.

M. Zare and I.A. Frigaard, “Pressure Reduction in Hydrating Cement Slurries” Poster presented at the Nordic Rheology Conference, June 13-15, 2018, Trondheim, Norway.

References:

Allouche, M., Frigaard, I.A., Sona, G. “Static wall layers in the displacement of two visco-plastic fluids in a plane channel." J. Fluid Mech., 424, 243-277, (2000).

Atherton E. Risk, D., Fougère, C., Lavoie, M., Marshall, A, Werring, J., Williams, J.P., Minions, C., “Mobile measurement of methane emissions from natural gas developments in Northeastern British Columbia, Canada” Atmos. Chem. Phys. 17(20), 12405-12420, (2017).

Bonett, A., Pafitis, D., “Getting to the root of gas migration.” Oilfield Review 8(1), 36-49, (1996).

Dusterhoft D. Wilson G., Newman, K., “Field Study on the use of cement pulsation to control gas migration”, SPE paper 75689-MS, 2002

Dusseault M.B., Jackson, R.E., MacDonald, D. “Towards a Road Map for Mitigating the Rates and Occurrences of Long-Term Wellbore Leakage.” Consulting report from Univ. Waterloo and Geofirma Engng. May 22, (2014).

Eslami, A., Frigaard, I.A., Taghavi, S.M. “Viscoplastic fluid displacement flows in horizontal channels: Numerical simulations.” J. Non-Newt. Fluid Mech. 249, 79-96 (2017).

Freitas, J.F., Soares, E.J., Thompson, R.L., “Immiscible Newtonian displacement by a viscoplastic material in a capillary plane channel." Rheol. Acta., 50(4), 403-422, (2011).

Freitas, J.F., Soares, E.J., Thompson, R.L. “Viscoplastic – viscoplastic displacement in a plane channel with interfacial tension effects." Chem. Engng. Sci., 91, 54-64, (2013).

Joseph, D.D., Renardy, Y.Y., “Fundamentals of Two-Fluid Dynamics. Part 2: Lubricated Transport, Drops and Miscible Liquids." Springer, volume 4, (1993).

Lajeunesse, E., Martin, J., Rakotomalala, N., Salin, D., Yortsos, Y.C., “Miscible displacement in a Hele-Shaw cell at high rates." J. Fluid Mech., 398, 299-319, (1999).

Moyers-Gonzalez, M., Frigaard, I.A., Nouar, C., “Nonlinear stability of a visco-plastically lubricated shear flow." J. Fluid Mech., 506, 117-146 (2004).

Nelson, E.B., Guillot, D., “Well Cementing.” 2nd Edition, Schlumberger Educational Services (2006)

Petitjeans, P., Maxworthy, T. “Miscible displacements in capillary tubes. Part 1. Experiments." J Fluid Mech., 326 (1996), pp. 37-56

Soares, E.J., Thompson, R.L. “Flow regimes for the immiscible liquid-liquid displacement in capillary tubes with complete wetting of the displaced liquid." J. Fluid Mech. 641, 63-84 (2009).

Wielage-Burchard, K., Frigaard, I.A., “Static wall layers in plane channel displacement flows." J. Non-Newtonian Fluid Mech., 166(5), 245-261, (2011).

M. Zare, A. Roustaei, K. Alba and I.A. Frigaard. “Invasion of fluids into a gelled fluid column: yield stress effects,” J. non-Newtonian Fluid Mechanics, 238, 212-223, (2016).

M. Zare, A. Roustaei, I.A. Frigaard. “Buoyancy effects on micro-annulus formation: Newtonian-Bingham fluid displacements in vertical channels.” J. non-Newtonian Fluid Mechanics, 247, 22-40, (2017).

M. Zare, I.A. Frigaard, “Onset of Miscible and Immiscible Fluids invasion into a Viscoplastic Fluid.” Physics of Fluids, accepted for publication and to appear in 2018.

M. Zare, I.A. Frigaard. “Buoyancy effects on micro-annulus formation: density unstable Newtonian-Bingham fluid displacements in vertical channels.” Submitted to J. non-Newtonian Fluid Mechanics, May 2018, under review.